J. Fluid Mech. (2023), *vol*. 963, A9, doi:10.1017/jfm.2023.300

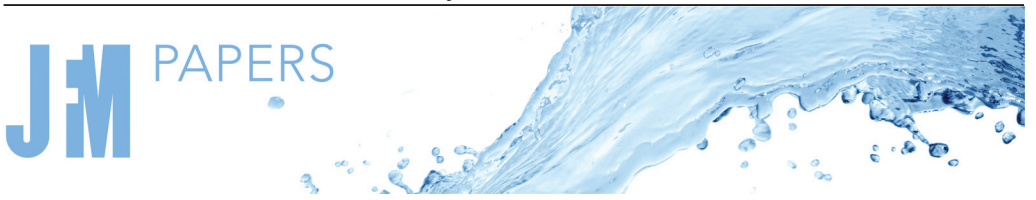

Magneto-gravity-elliptic instability

Abdelaziz Salhi[1,2,†] **and Claude Cambon**[2]

[1]Département de Physique, Faculté des Sciences de Tunis, Université Tunis El Manar, 2092 El Manar, Tunis, Tunisia

[2]Université de Lyon, Laboratoire de Mécanique des Fluides et d'Acoustique, UMR 5509, Ecole Centrale de Lyon, CNRS, UCBL, INSA, F-69134 Ecully CEDEX, France

(Received 6 January 2023; revised 8 March 2023; accepted 3 April 2023)

Magneto-gravity-elliptic instability is addressed here considering an unbounded strained vortex (with constant vorticity 2Ω and with ellipticity parameter ε) of a perfectly conducting fluid subjected to a uniform axial magnetic field (with Alfvén velocity scaled from the basic magnetic field B) and an axial stratification (with a constant Brunt–Väisälä frequency N). Such a simple model allows us to formulate the stability problem as a system of equations for disturbances in terms of Lagrangian Fourier (or Kelvin) modes which is universal for wavelengths of the perturbation sufficiently small with respect to the scale of variation of the basic velocity gradients. It can model localised patches of elliptic streamlines which often appear in some astrophysical flows (stars, planets and accretion discs) that are tidally deformed through gravitational interaction with other bodies. In the limit case where the flow streamlines are exactly circular ($\varepsilon = 0$), there are fast and slow magneto-inertia-gravity waves with frequencies $\omega_{1,2}$ and $\omega_{3,4}$, respectively. Under the effect of finite ellipticity, the resonant cases of these waves, $\omega_i - \omega_j = n\Omega$ $(i \neq j)$ (n being an integer), can become destabilising. The maximal growth rate of the subharmonic instability (related to the resonance of order $n = 2$) is determined by extending the asymptotic method by Lebovitz & Zweibel (*Astrophys. J.*, vol. 609, 2004, pp. 301–312). The domains of the $(k_0B/\Omega, N/\Omega)$ plane for which this instability operates are identified ($1/k_0$ being a characteristic length scale). We demonstrate that the $N \to 0$ limit is, in fact, singular (discontinuous). The axial stable stratification enhances the subharmonic instability related to the resonance between two slow modes because, at large magnetic field strengths, its maximal growth rate is twice that found in the case without stratification.

Key words: parametric instability, stratified flows

1. Introduction

The three-dimensional (3D) elliptical flow instability is very generic and occurs in many flow configurations, when the basic velocity field (or base flow) consists of large horizontal

† Email address for correspondence: lazizsalhi@yahoo.fr

vortices with elliptical streamlines in their core. The elliptic instability is a parametric resonance of internal (usually inertial) waves due to an elliptical deformation of the streamlines of a rotating flow. The reader is referred to Kerswell (2002) for a detailed review and references therein. The origin of the ellipticity in the core of eddies is multifold. In the study of the stability of airplane wakes, we have to consider the presence, before their possible breaking, of a pair of large counter-rotating vortices: this is the mutual induction of these eddies that render their core elliptic. More generally, the characteristics and behaviour of counter-rotating and corotating vortex pairs have been recently reviewed in the study by Leweke, Le Dizes & Williamson (2016).

In line with former studies, McKeown *et al.* (2020) showed that iterations of the elliptical instability, arising from the interactions between counter-rotating vortices, lead to the emergence of turbulence. As a second example, in rotating flows subjected to precession, the gyroscopic torque, mediated by the misalignment of solid-body rotation and system angular velocity, induces an additional shear that, superimposed to solid-body rotation, results in elliptical streamlines, as shown by Kerswell (1993*a*) and by Salhi & Cambon (2009) in the simplest geometry. More generally, elliptical shape caused by tidal forces is very common in many astrophysical systems such as planetary cores, binary stars, gaseous planets and accretion discs. The importance of elliptical instability, in a purely hydrodynamic context, in the tidal dissipation mechanism in such astrophysical systems has been the subject of several studies in the literature (Barker & Lithwick 2013; Cébron *et al.* 2013; Barker 2016; Barker, Braviner & Ogilvie 2016). Note that tidal dissipation generates heat in astrophysical systems, which in some cases may be important for their structure and evolution (Ogilvie 2014).

Being the ellipticity due to the mutual induction of adjacent vortices or not, the elliptical instability is local, so that it is generally sufficient to consider a single elliptic eddy for the base (or mean) flow. For trailing vortices again, it has been shown that the Moore–Saffman–Tsai–Widnall (MSTW) instability (Moore & Saffman 1975; Tsai & Widnall 1976), in the short-wavelength regime, is an elliptical instability (Éloy & Le Dizes 2001; Fukumoto 2003; Sipp & Jacquin 2003; Chang & Smith 2021). It is worth mentioning that the MSTW instability encompasses the long-wave instability bearing with Crow's instability (Crow 1970) which occurs through the mutual induction of a pair of parallel counter-rotating vortex columns (McKeown *et al.* 2020): the Biot–Savart law is generally used to compute the induced velocity on one of the trailing vortices owing to the presence of the other. Recently, Feys & Maslowe (2016) have examined the elliptical instability of the Moore and Saffman model Moore & Saffman (1975) for a *single* trailing vortex. Their results demonstrate the significant effect of the distribution and intensity of the axial flow on the elliptical instability of a trailing vortex. Such a robust 3D instability leads to vortex decay under most circumstances, as reviewed by Lesur & Papaloizou (2009). Rather old experimental evidences are quoted in the following historical review, and recently the nonlinear fate of libration-induced elliptical instability in low-dissipation and low-forcing regimes has been explored experimentally by Le Reun, Favier & Le Bars (2019). They showed that once the saturation of the elliptical instability is reached, a turbulent state is observed for which the energy is injected only in the resonant inertial waves.

It is clear that the elliptical instability has a very long history, and deserves a survey, as follows. This allows us to discuss what is the simplest mathematical way to identify it and to quantify its effects, first in the neutral (non-stratified), purely hydrodynamical case. After some experimental evidences of that instability (Gledzer *et al.* 1975; Malkus 1989), see also the recent review by McKeown *et al.* (2020), a sudden interest arose when Pierrehumbert (1986) discovered its characteristic properties by a conventional normal

mode analysis approach, whereas at the same time Bayly (1986) found the same results using the simpler and more elegant method using Kelvin modes, or mean-flow-advected (Lagrangian) Fourier modes along elliptical trajectories. The latter study, similar to that by Craik & Criminale (1986), was foreshadowed by a rapid distortion theory (RDT) analysis by Cambon (1982), and Cambon, Teissedre & Jeandel (1985) (in French). This is re-discussed, in English, by Godeferd, Cambon & Leblanc (2001), with especially its figure 3, and in Sagaut & Cambon (2008) for a recent overview. Waleffe (1989, 1990) clearly described the physical mechanism of the elliptical instability as a vortex stretching mechanism and showed how the growing Kelvin modes found by Bayly (1986) in the case of unbounded strained vortex could be superimposed to create a localised, unstable disturbance of the form found in the bounded elliptical cylinder case (Gledzer *et al.* 1975).

From the previous studies, let us summarise the advantages of the formalism with projection of the disturbance fields onto Kelvin modes. The Kelvin modes are essentially 3D Fourier modes, even if the wave vector can become time-dependent following the mean flow streamlines. The time dependency of the wave vector represents the convection of the plane wave $\exp(\mathrm{i}\boldsymbol{k}(t)\cdot\boldsymbol{x})$ by the base flow. Both the direction and magnitude of $\boldsymbol{k}$ change as wave crests rotate and approach or separate from each other due to basic velocity gradients. Accordingly, all the formal advantages of Fourier space remain valid: pure algebraic formulation of integro-differential equations, including Poisson equation for pressure disturbances, algebraic dissipation term instead of Laplacian operator, algebraic linkage from vorticity to velocity (instead of a Biot–Savart relationship). It is worth emphasising that the system of equations for disturbances in terms of Lagrangian Fourier modes is universal under a typical length scale. Indeed, such a system is recovered for small-scale disturbances traveling near any smooth base-flow trajectory, in the zonal asymptotic method of Lifschitz & Hameiri (1991) with close connection with geometric optics; the velocity gradients of the base flow are treated as space-uniform in a domain of unspecified length scale, asymptotically small (see also Godeferd *et al.* 2001).

Can the elliptic instability, in the pure hydrodynamic context, survive in the presence of vertical basic density stratification, that is stabilising considered alone? A first answer is given by the study of the stability of inertia-gravity waves when it is altered by the ellipticity of streamlines. In relation to the dynamics of ocean and atmosphere (Miyazaki & Fukumoto 1992; Miyazaki 1993) investigated the influence of the Coriolis force and density stratification, caused by temperature or salinity gradient, on the elliptical instability. Miyazaki & Fukumoto (1992) considered an unbounded strained-vortex flow with stable axial stratification. They have found that the growth rates for the elliptical instability were invariably reduced: the subharmonic elliptical instability is completely suppressed when Brunt–Väisälä frequency (N) is greater or equal to the half of the basic vorticity strength (Ω). For small eccentricities, asymptotic theory leads to formulae for the maximum growth rate (Kerswell 2002) (see also § 3 in the present study). It is worth mentioning that the elliptical instability of stratified vortices has been addressed as well in previous studies (Otheguy, Chomaz & Billant 2006; Le Bars & Le Dizès 2006; Guimbard *et al.* 2010; Suzuki, Hirota & Hattori 2018). The effects of differential diffusion between momentum and density on the elliptical instability have recently been addressed by Singh & Mathur (2019). They showed that, in the case where the ratio of thermal diffusivity to kinematic diffusivity is equal to unity, the viscous effects are purely suppressive, whereas for sufficiently small values of this ratio, there is an oscillatory instability whose signature is nevertheless present with zero growth rate in the inviscid limit. In turbulent Rayleigh–Bénard convection, Zwirner, Tilgner & Shishkina (2020) showed that the mechanism which causes the twisting and breaking of a single-roll

large-scale circulation into multiple rolls is the elliptical instability. On the other hand, density effects on the MSTW instability have been recently investigated by Chang & Smith (2021) who performed a normal mode stability analysis and showed that, for the subharmonic instability (resonance $(m, m+2) = (0, 2)$, m being the azimuthal wavenumber) the growth rate is maximised when the ratio of vortex to ambient fluid density is near 0.215.

The interaction of vortices with a magnetic field is a fundamental process in astrophysical magnetohydrodynamics (MHD). Therefore, a similar question occurs when one moves from hydrodynamics to MHD when the electrically conducting elliptical flow is subjected to an unperturbed (or a basic) magnetic field. In a geophysical context, Kerswell (1994) studied the effect of a toroidal magnetic field on the elliptic instability in a rotating spheroidal container filled with an incompressible electrically conducting fluid, which carries a constant axial electric current. He concluded that the toroidal magnetic field has a stabilising influence. By including the effect of a uniform magnetic field perpendicular to the plane of the elliptical base flow, the resulting magneto-elliptic instability has been related to the problem of turbulence generation and, hence, momentum transport in accretion discs by Lebovitz & Zweibel (2004) (hereafter LZ04). In that study, an analytical technique was developed to determine the maximal growth rates of the destabilising resonances of order $n = 2$ (i.e. subharmonic instabilities, see (1.1)) in the limit of small elliptical (tidal) deformations. This analytical technique has been used in previous studies by Mizerski & Bajer (2009) for the magneto-elliptical instability of rotating systems and by Salhi, Lehner & Cambon (2010) for the magneto-precessional instability. Herreman *et al.* (2010) conducted experiments to explain some aspects of the nonlinear transition process for the elliptic instability in rotating cylinders under imposed magnetic field. It is worth noting that in the case where the Coriolis and Lorentz forces are simultaneously present and when the wave vector $\boldsymbol{k}$ aligns with the magnetic field the elliptical flow can develop horizontal instability which dominates over all other modes (Bajer & Mizerski 2013). In the astrophysical context (tidal dissipation in gaseous planets and stars), Barker & Lithwick (2014) found that magnetic fields do prevent vortices from forming and, hence, greatly enhance the steady-state dissipation rate.

The combined effects of stable density stratification and MHD on the elliptical instability within an elliptically distorted cylinder have been investigated by Kerswell (1993*b*). He performed a normal mode stability analysis for a simple configuration possessing considerable symmetry between the velocity and magnetic fields: a purely azimuthal magnetic field, which in the frozen flux limit is also elliptically distorted. In that study, stratification is either axial (the isopycnics are parallel to the streamlines) or radial (the isopycnics are perpendicular to the streamlines).

In the present paper we analyse in detail the joint influence of a stable axial stratification (with strength N) and an external (axial) uniform magnetic field (with Alfvén velocity scaled from the basic magnetic field B) on the stability of an unbounded flow with elliptical streamlines of a perfectly conducting fluid. Our study extends the study by Miyazaki & Fukumoto (1992) by including the effects of a magnetic field and also the study by LZ04 by including the effects of an axial stable stratification. An important aspect of the present study is to map out the regime of $(B/(L_0\Omega), N/\Omega)$ space (L_0 being a characteristic length scale) for which the destabilising resonances of order $n = 2$ (see (1.1)) of magneto-inertia-gravity (MIG) waves prone to operate and to determine their growth rates at small ellipticity by extending the analytical technique by LZ04. In the laboratory experiment of a magnetised turbulent Taylor–Couette flow of liquid metal by Nornberg *et al.* (2010), the combined fast and slow Alfvén-inertial waves were clearly identified

where the observed slow wave is damped. These authors have identified a relationship between the slow magneto-inertial waves and the magneto-rotational instability (MRI) (Balbus & Hawley 1991; Wang *et al.* 2022). On the other hand, Mizerski & Lyra (2012) examined the link between the magneto-elliptical instability and the MRI, explaining that the two instabilities are different manifestations of the same magneto-elliptical-rotational instability. Salhi *et al.* (2012) have studied the effects of stable stratification on the MRI instability and showed that, under the MHD Boussinesq approximation (e.g. Wilczyński, Hughes & Kersalé 2022), the so-called 'magnetic induction potential scalar' (MIPS, i.e. the scalar product of the magnetic field vector and the density gradient) is a Lagrangian invariant for a non-diffusive fluid. In contrast, the potential vorticity (PV), which is very useful as an invariant in stratified geophysical flows (e.g. Pedlosky 2013), is no longer valid in MHD because it removes the baroclinic torque in the extended vorticity equation, but not the counterpart of the Lorentz force.

An asymptotic stability analysis is developed in § 3 at leading order in the ellipticity parameter ε in order to determine the growth rates of the (subharmonic) instability tongues that emanate from the points at vanishing ellipticity. In this limit, disturbances to the basic flow are found in terms of MIG dispersive waves, with a dispersion law (Salhi *et al.* 2017) that includes Ω, N, B/L_0 and the angular parameter $\mu = \cos(\theta)$ (the angle θ being the angle between the wave vector of the perturbations and that of the base-flow vorticity). In contrast with particular cases, the general dispersion law of MIG waves is no longer a simple combination of the individual dispersion frequencies, considered alone, but is obtained in combining the eigenvalues of the matrix of the whole linear system of equations (Salhi *et al.* 2017). Fast and slow modes are identified, with different resonance conditions between them, or

$$\omega_i - \omega_j = n\Omega \quad (i, j = 1, 2, 3, 4,\ i \neq j,\ n \text{ being an integer}). \tag{1.1}$$

Without an analysis of the resonant conditions, it is not possible to simply identify the different instabilities, namely if they are subharmonic or not, if they result from the interaction of two fast modes, two slow modes, or one fast and one slow.

As detailed in § 2, the use of the *magnetic invariant* (MIPS) makes it possible to reduce the linear system of ordinary differential equations, which represents a Floquet problem, from a five-component system to a four-component system only. In § 3, we show that stable stratification enhances the destabilising resonance of order $n = 2$ between two slow modes because we find that, at large magnetic strengths, its growth rate is about twice that found in the case without stratification (LZ04). Asymptotic formulae are compared with numerical results carried out at arbitrary ellipticity in § 4. The effect of diffusion is briefly addressed in the special case where the diffusion coefficients (kinetic, thermal and magnetic) are equal. Conclusions and perspectives are offered in § 5.

2. MHD Boussinesq's equations

We consider a stratified electrically conducting fluid. Density variations are introduced using the Boussinesq approximation for simplicity (Chandrasekhar 1961). The fluid is assumed to be inviscid and non-diffusive. The effect of viscosity (ν) and thermal (κ) and magnetic (η) diffusivity are briefly addressed in § 4.3 by considering the case where $\nu = \kappa = \eta$ (i.e. the case where the magnetic and thermal Prandtl numbers are unity).

The Boussinesq MHD equations written in a fixed frame take the form (Davidson 2013)

$$D_t\tilde{\boldsymbol{u}} = -\boldsymbol{\nabla}\tilde{p} + \left(\tilde{\boldsymbol{b}}\cdot\boldsymbol{\nabla}\right)\tilde{\boldsymbol{b}} + \tilde{\vartheta}\boldsymbol{n} + \nu\nabla^2\tilde{\boldsymbol{u}}, \tag{2.1a}$$

$$D_t\tilde{\boldsymbol{b}} = \left(\tilde{\boldsymbol{b}}\cdot\boldsymbol{\nabla}\right)\tilde{\boldsymbol{u}} + \eta\nabla^2\tilde{\boldsymbol{b}}, \tag{2.1b}$$

$$D_t\tilde{\vartheta} = \kappa\nabla^2\tilde{\vartheta}, \tag{2.1c}$$

$$\boldsymbol{\nabla}\cdot\tilde{\boldsymbol{u}} = 0, \tag{2.1d}$$

$$\boldsymbol{\nabla}\cdot\tilde{\boldsymbol{b}} = 0, \tag{2.1e}$$

where $D_t(\cdot) \equiv (\partial_t + \tilde{\boldsymbol{u}}\cdot\boldsymbol{\nabla})(\cdot)$ denotes the material derivative, $\tilde{\boldsymbol{u}}$ denotes the velocity and $\tilde{\boldsymbol{b}}$ denotes the magnetic field which is scaled using Alfvén velocity units, i.e. it is divided by $\sqrt{\rho_0\mu_0}$ where ρ_0 and μ_0 are the constant density and the magnetic permeability of the fluid. Here, $\tilde{p}$ being the total pressure (including the magnetic part) divided by the constant density ρ_0. In the present study, we consider axial stratification,

$$\boldsymbol{n} = \boldsymbol{e}_3 = -\boldsymbol{g}/g. \tag{2.2}$$

where $\boldsymbol{e}_3$ is the upward vertical unit vector and $\boldsymbol{g}$ is the gravitational acceleration vector. The first equation in the above system is the momentum equation, the second is the induction equation for the magnetic field and the third is the buoyancy scalar equation. Both velocity field and magnetic field are solenoidal (2.1*d*,*e*).

For a non-magnetised Boussinesq ideal fluid, one may easily show that the PV (Pedlosky 2013),

$$\tilde{\varpi}_\kappa = \tilde{\boldsymbol{\omega}}_a\cdot\boldsymbol{\nabla}\tilde{\vartheta}, \tag{2.3}$$

is a Lagrangian, invariant, i.e. $D_t\tilde{\varpi}_\kappa = 0$. Here, $\tilde{\boldsymbol{\omega}}_a$ is the absolute vorticity vector which, in the absence of the Coriolis force, identifies with the vorticity vector $\boldsymbol{W} = \boldsymbol{\nabla}\times\tilde{\boldsymbol{u}}$. A counterpart, for a magnetised Boussinesq ideal fluid, is the so-called MIPS (Salhi *et al.* 2012)

$$\tilde{\varpi}_m = \tilde{\boldsymbol{b}}\cdot\boldsymbol{\nabla}\tilde{\vartheta} \tag{2.4}$$

that is a Lagrangian invariant, i.e. $D_t\tilde{\varpi}_m = 0$, and not $\tilde{\varpi}_\kappa$. The usefulness of introducing the MIPS is illustrated later.

2.1. *Base flow*

The solutions of system (2.1) are conveniently decomposed into a 'basic flow' $(\boldsymbol{U}, P, \boldsymbol{B}, \Theta)$ and a 'disturbance' $(\boldsymbol{u}, p, \boldsymbol{b}, \vartheta)$, but the latter needs to be small compared with the former,

$$\tilde{\boldsymbol{u}} = \boldsymbol{U} + \boldsymbol{u}, \quad \tilde{p} = P + p, \quad \tilde{\boldsymbol{b}} = \boldsymbol{B} + \boldsymbol{b}, \quad \tilde{\vartheta} = \Theta + \vartheta. \tag{2.5a–d}$$

We consider the linear stability of a stratified vortical flow with elliptical streamlines and with uniform vertical magnetic field (see figure 1)

$$\boldsymbol{U} = \boldsymbol{A}\cdot\boldsymbol{x}, \quad \boldsymbol{A} = \Omega\begin{pmatrix} 0 & -E & 0 \\ E^{-1} & 0 & 0 \\ 0 & 0 & 0 \end{pmatrix} \tag{2.6a}$$

$$\boldsymbol{B} = B\boldsymbol{e}_3, \tag{2.6b}$$

$$\Theta = N^2 x_3 \tag{2.6c}$$

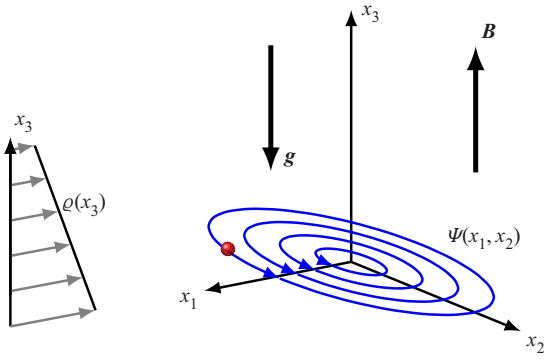

Figure 1. A schematic drawing of the basic state: planar flow with elliptical streamlines, $\Psi = -(\Omega/2)(E^{-1}x_1^2 + Ex_2^2)$ being the stream function in the presence of an axial uniform magnetic field ($\boldsymbol{B} = B\boldsymbol{e}_3$) and an axial stable stratification ($\Theta = N^2 x_3$, $N^2 = -(g/\rho_0)(\mathrm{d}\varrho/\mathrm{d}x_3)$, N being the Brunt–Väisälä frequency). The gravity vector is given by $\boldsymbol{g} = -g\boldsymbol{e}_3$ with $g > 0$.

where Ω is a constant that is a measure of the intensity of the flow and $E \geq 1$ is a measure of elliptical deformation of the streamlines, and N is the Brunt–Väisälä frequency such that

$$N^2 = -\frac{g}{\rho_0}\frac{\mathrm{d}\varrho}{\mathrm{d}x_3}. \tag{2.7}$$

Circular streamlines correspond to the case where $E = 1$. The parameter

$$\varepsilon = \tfrac{1}{2}\left(E - E^{-1}\right) \tag{2.8}$$

represents the departure of the streamlines of the unperturbed flow from axial symmetry. We note that

$$0 < \delta = (E - E^{-1})/(E + E^{-1}) < 1 \tag{2.9}$$

for the flow to be elliptical. We also note that, an equivalent form for the unperturbed velocity field has been used in previous studies (Waleffe 1990; Miyazaki & Fukumoto 1992; Miyazaki 1993; Kerswell 2002; Mizerski & Bajer 2009; Bajer & Mizerski 2013)

$$\boldsymbol{U} = \Gamma\left[-(1+\delta)\,x_2\boldsymbol{e}_1 + (1-\delta)\,x_1\boldsymbol{e}_2\right], \tag{2.10}$$

where $2\Gamma = \Omega(E + E^{-1})$ and $-\Gamma\delta$ represents the strain rate, but the expression (2.6*a*) seems more suitable for analysing resonant destabilisation (Mizerski & Bajer 2009).

The basic buoyancy scalar Θ varies linearly with the axial coordinate x_3 (axial stratification) and is proportional to the gravitational acceleration, g, and to a background density (or temperature) gradient. This linear profile admits a constant Brunt–Väisälä frequency N throughout the entire fluid. More general exact solutions of the combined stratified fluid/magnetic equations exist in an unbounded domain (Craik 1989); the case in hand (i.e. (2.6)) is probably the simplest of these. As indicated previously, Miyazaki & Fukumoto (1992) considered an unbounded strained-vortex flow with stable exponential stratification in the axial direction at small Froude number, $Fr = \Gamma^2 L_0/g \ll 1$ with L_0 a characteristic length scale. One may show that the resulting linear differential system for the disturbances superimposed on the base flow is the same considering either an exponential basic stratification or a linear (with respect to space coordinates) basic stratification. Both profiles (exponential or linear) admit a constant Brunt–Väisälä frequency throughout the entire fluid.

2.2. *Perturbed system*

In the following, we consider the case of a non-diffusive fluid. Diffusivity effects with the assumption that the diffusion coefficients are equal ($\nu = \kappa = \eta$) or, equivalently, the magnetic and thermal Prandtl numbers are equal to one are briefly discussed at the end of § 4.

2.2.1. *Linearised system in physical space*

We substitute the solutions (2.5*a–d*) into the system (2.1) and linearise. Linearisation is not readily justified by the fact that the flow disturbances are very small with respect to the base flow. Linearisation is briefly discussed in the conclusion. Thus, we expect our analysis to break down when the disturbances become so large that nonlinear effects become important. The resulting perturbed equations are

$$D_t \boldsymbol{u} = -\boldsymbol{\nabla} p - (\boldsymbol{u}\cdot\boldsymbol{\nabla})\,\boldsymbol{U} + (\boldsymbol{B}\cdot\boldsymbol{\nabla})\,\boldsymbol{b} + \vartheta \boldsymbol{e}_3, \tag{2.11a}$$

$$D_t \boldsymbol{b} = (\boldsymbol{b}\cdot\boldsymbol{\nabla})\,\boldsymbol{U} + (\boldsymbol{B}\cdot\boldsymbol{\nabla})\,\boldsymbol{u}, \tag{2.11b}$$

$$D_t \vartheta = -N^2 u_3, \tag{2.11c}$$

$$\boldsymbol{\nabla}\cdot\boldsymbol{u} = 0, \tag{2.11d}$$

$$\boldsymbol{\nabla}\cdot\boldsymbol{b} = 0. \tag{2.11e}$$

As for the linear part of MIPS (see (2.4)), it takes the form

$$\varpi_m = B\frac{\partial \vartheta}{\partial x_3} + N^2 b_3, \tag{2.12}$$

where $D_t \varpi_m = 0$, so that $\varpi_m = \text{const}$. As shown later, for the purposes of studying stability, we may set $\varpi_m = 0$ (see also Benkacem *et al.* 2022).

2.2.2. *Floquet system in wave space*

The disturbances are expressed in terms of Lagrangian Fourier modes, as discussed in section 1. These modes were used for shear waves by Moffatt (2010), who was probably the first to call them 'Kelvin modes', in reference to a pioneering paper by Lord Kelvin Kelvin (1887) in the nineteenth century. They are advected by the mean flow as Lagrangian invariants (Cambon 1982; Sagaut & Cambon 2008), as plane waves for which the direction and the speed of propagation depend on time, via a time-dependent wave vector:

$$\left[\boldsymbol{u}, p, \boldsymbol{b}, \vartheta\right](\boldsymbol{x}, t) = \left[\hat{\boldsymbol{u}}, \hat{p}, \hat{\boldsymbol{b}}, \hat{\vartheta}\right](\boldsymbol{k}, t)\exp\left(\mathrm{i}\boldsymbol{x}\cdot\boldsymbol{k}(t)\right), \tag{2.13}$$

where $\mathrm{i}^2 = -1$. Accordingly, the material derivative of the fluctuating velocity can be rewritten as

$$D_t \boldsymbol{u} = \left(\partial_t + U_j\frac{\partial}{\partial x_j}\right)\left[\hat{\boldsymbol{u}}(\boldsymbol{k}, t)\exp\left(\mathrm{i}\boldsymbol{x}\cdot\boldsymbol{k}(t)\right)\right] \tag{2.14}$$

with $U_j = A_{jm}x_m$, so that

$$D_t \boldsymbol{u} = \left[\partial_t \hat{\boldsymbol{u}} + \mathrm{i}\left((d_t k_j)x_j + A_{jm}k_j x_m\right)\hat{\boldsymbol{u}}\right]\exp\left(\mathrm{i}\boldsymbol{x}\cdot\boldsymbol{k}(t)\right), \tag{2.15}$$

or, equivalently,

$$D_t \boldsymbol{u} = \left(\partial_t \hat{\boldsymbol{u}} + \mathrm{i}\left[\left(d_t\boldsymbol{k} + A^T\boldsymbol{k}\right)\cdot\boldsymbol{x}\right]\hat{\boldsymbol{u}}\right)\exp\left(\mathrm{i}\boldsymbol{x}\cdot\boldsymbol{k}(t)\right). \tag{2.16}$$

In order to remove the explicit dependence on $\boldsymbol{x}$ in the resulting equations for the Fourier amplitudes $\hat{\boldsymbol{u}}$, $\hat{\boldsymbol{b}}$, $\hat{p}$ and $\hat{\vartheta}$, one has to ensure that $\boldsymbol{k}(t)$ varies in time according to the eikonal equation

$$d_t \boldsymbol{k} = -\boldsymbol{A}^T \cdot \boldsymbol{k}, \tag{2.17}$$

where $d_t(\cdot) \equiv \mathrm{d}(\cdot)/\mathrm{d}t$ and T denotes transpose. Equation (2.17) can be solved to give

$$k_1 = k_p \cos(\tau - \phi), \quad k_2 = E k_p \sin(\tau - \phi), \quad k_3 = k_{30}, \tag{2.18a–c}$$

where $\tau = \Omega t$ being a dimensionless time,

$$k_p^2 = k_1^2 + E^{-2} k_2^2 = k_{10}^2 + E^{-2} k_{20}^2, \quad \tan\phi = -E^{-1} k_{20}/k_{10}, \tag{2.19a,b}$$

with k_{j0} ($j = 1, 2, 3$) the initial wave vector component. For purposes of studying stability, we may set $\phi = 0$. This is easily seen by making the substitution $\Omega t' = \Omega t + \phi$, which eliminates ϕ from the equation.

Substituting the plane waves solution (2.13) into the system (2.11) and taking into account the eikonal equation (2.17), we obtain

$$d_t \hat{\boldsymbol{u}} = -\mathrm{i}\hat{p}\boldsymbol{k} - \boldsymbol{A} \cdot \hat{\boldsymbol{u}} + \mathrm{i}\,(k_3 B)\,\hat{\boldsymbol{b}} + \hat{\vartheta}\boldsymbol{e}_3, \tag{2.20a}$$

$$d_t \hat{\boldsymbol{b}} = \boldsymbol{A} \cdot \hat{\boldsymbol{b}} + \mathrm{i}\,(k_3 B)\,\hat{\boldsymbol{u}}, \tag{2.20b}$$

$$d_t \hat{\vartheta} = -N^2 \hat{u}_3, \tag{2.20c}$$

together with $\boldsymbol{k} \cdot \hat{\boldsymbol{u}} = 0$ and $\boldsymbol{k} \cdot \hat{\boldsymbol{b}} = 0$. The use of the latter conditions allows one to eliminate the Fourier amplitude of fluctuating pressure,

$$\hat{p}(\boldsymbol{k}, t) = -\mathrm{i}k^{-2}\left(2\Omega^2 \hat{c}_1 + k_3 \hat{\vartheta}\right), \quad \Omega \hat{c}_1 = E k_1 \hat{u}_2 - E^{-1} k_2 \hat{u}_1, \tag{2.21a,b}$$

and to reduce the above seven-component Floquet system to a five-component version. Here, $k = \sqrt{k_1^2 + k_2^2 + k_3^2}$ is the modulus of the wave vector. This reduction of components results from the fact that both Fourier modes for fluctuating velocity and for fluctuating magnetic field are two-component in the plane normal to the wave vector. Such projection can be done using the orthonormal Craya–Herring frame of reference, as used in several articles (e.g.from Salhi & Cambon 1997).

We note that the case where the wave vector is vertical, so that $k_1 = k_2 = 0$, $k_p = 0$ and $k_3 = \pm k$, characterises a special class of disturbances, called horizontal perturbations, in which the vertical components $\hat{u}_3$ and $\hat{b}_3$ identically vanish (Bajer & Mizerski 2013). In that case, axial stratification has no effect on the horizontal perturbations, and then there is no instability without the Coriolis force.

2.2.3. *Change of variables*

At $k_3 = 0$, the solution of the resulting Floquet system (2.20) is stable. Accordingly, we henceforth consider only perturbations with vertical wave number $k_3 \neq 0$. As in the studies by LZ04 and by Mizerski & Bajer (2009), we transform the resulting Floquet system in

terms of the following variables to facilitate subsequent calculations

$$\Omega\hat{c}_2 = -k_3\hat{u}_3, \quad \Omega\hat{c}_3 = Ek_1\hat{b}_2 - E^{-1}k_2\hat{b}_1, \quad \Omega\hat{c}_4 = -k_3\hat{b}_3, \quad \Omega^2\hat{c}_5 = -k_3\hat{\vartheta}. \tag{2.22a–d}$$

Given (2.21*a*,*b*) we transform the system (2.20) according to these new variables,

$$d_\tau\hat{c}_1 = -4\varepsilon\frac{k_1k_2}{k^2}\hat{c}_1 - 2\hat{c}_2 + \mathrm{i}\frac{(k_3B)}{\Omega}\hat{c}_3 + 2\varepsilon\frac{k_1k_2}{k^2}\hat{c}_5, \tag{2.23a}$$

$$d_\tau\hat{c}_2 = 2\frac{k_3^2}{k^2}\hat{c}_1 + \mathrm{i}\frac{(k_3B)}{\Omega}\hat{c}_4 + \frac{k_\perp^2}{k^2}\hat{c}_5, \tag{2.23b}$$

$$d_\tau\hat{c}_3 = \mathrm{i}\frac{(k_3B)}{\Omega}\hat{c}_1, \tag{2.23c}$$

$$d_\tau\hat{c}_4 = \mathrm{i}\frac{(k_3B)}{\Omega}\hat{c}_2, \tag{2.23d}$$

$$d_\tau\hat{c}_5 = -\frac{N^2}{\Omega^2}\hat{c}_2, \tag{2.23e}$$

where $d_\tau\hat{c}_1 = \Omega^{-1}d_t\hat{c}_1$ and $k_\perp = \sqrt{k_1^2 + k_2^2}$. Combining (2.23*d*) and (2.23*e*), we deduce the following relation:

$$-\frac{\Omega}{k_3}\left[\mathrm{i}\Omega\,(k_3B)\,\hat{c}_5 + N^2\hat{c}_4\right] = \mathrm{i}\,(k_3B)\,\hat{\vartheta} + N^2\hat{b}_3 = \hat{\varpi}_m = \text{const.}, \tag{2.24}$$

which represents the spectral counterpart of the MIPS (see (2.4)). Accordingly, system (2.23) can be further reduced to a fourth-order inhomogeneous Floquet system,

$$d_\tau\hat{\boldsymbol{c}} = \boldsymbol{D}(\tau)\cdot\hat{\boldsymbol{c}} + \hat{\boldsymbol{\varphi}}, \tag{2.25}$$

where the only non-zero elements of $\boldsymbol{D}(\tau)$ are

$$D_{11} = -4\varepsilon\frac{k_1k_2}{k^2}, \quad D_{12} = -2, \quad D_{21} = 2\frac{k_3^2}{k^2}, \tag{2.26a}$$

$$D_{13} = D_{31} = D_{42} = \mathrm{i}\frac{(k_3B)}{\Omega}, \tag{2.26b}$$

$$D_{14} = 2\mathrm{i}\varepsilon\frac{N^2}{\Omega\,(k_3B)}\frac{k_1k_2}{k^2}, \tag{2.26c}$$

$$D_{24} = \mathrm{i}\left(\frac{(k_3B)}{\Omega} + \frac{N^2}{\Omega\,(k_3B)}\frac{k_\perp^2}{k^2}\right). \tag{2.26d}$$

The non-zero components of the inhomogeneous term in (2.25) take the form

$$\hat{\varphi}_1 = 2\mathrm{i}\varepsilon\frac{k_1k_2}{k^2}\frac{\hat{\varpi}_m}{(\Omega^2B)}, \tag{2.27a}$$

$$\hat{\varphi}_2 = \mathrm{i}\frac{k_\perp^2}{k^2}\frac{\hat{\varpi}_m}{(\Omega^2B)} \tag{2.27b}$$

and it can be seen as a time-varying forcing excitation.

Note that in the non-magnetised stratified case, one can use the fact that the PV is a Lagrangian invariant for a non-diffusive fluid (Pedlosky 2013) to derive a non-homogeneous two-component Floquet system in terms of the variables $\hat{c}_1$ and $\hat{c}_2$.

2.3. *Homogeneous Floquet system*

The linear system (2.25) has the properties $\boldsymbol{D}(\tau + T) = \boldsymbol{D}(\tau)$ and $\hat{\boldsymbol{\varphi}}(\tau + T) = \hat{\boldsymbol{\varphi}}(\tau)$ where $T = 2\pi$ is the period common to both the matrix $\boldsymbol{D}$ and the vector $\hat{\boldsymbol{\varphi}}$. Floquet theory does not address stability of the inhomogeneous system described by (2.25) where the 'forcing excitation' $\hat{\boldsymbol{\varphi}}(\tau)$ is present. However, the T-periodic nature of $\hat{\boldsymbol{\varphi}}(\tau)$ allows an extension to the theory (Slane & Tragesser 2011). Following the study of Slane & Tragesser (2011), it is shown that the basic behaviour of the homogeneous system

$$d_\tau \hat{\boldsymbol{c}} = \boldsymbol{D} \cdot \hat{\boldsymbol{c}} \tag{2.28}$$

does not change with the addition of the term $\hat{\boldsymbol{\varphi}}(\tau)$. Here, $\hat{\boldsymbol{c}} = (\hat{c}_1, \hat{c}_2, \hat{c}_3, \hat{c}_4)^{\mathrm{T}}$ in the canonical basis of $\mathbb{C}^4$. In other words, for purposes of studying stability, one may set $\hat{\varpi}_\kappa = 0$, so that $\hat{\boldsymbol{\varphi}} = \boldsymbol{0}$ (Benkacem *et al.* 2022).

We denote by $\boldsymbol{\Phi}(\tau)$ any fundamental matrix solution of the homogeneous system (2.28) where $\boldsymbol{\Phi}(0) = \boldsymbol{I}_4$. According to Floquet–Lyapunov theorem, $\boldsymbol{\Phi}$ is expressible in the form (Kuchment 1993),

$$\boldsymbol{\Phi}(\tau) = \boldsymbol{F}(\tau) \exp(\boldsymbol{K}\tau), \tag{2.29}$$

where $\boldsymbol{F}(\tau)$ is a non-singular continuous 2π-periodic 4×4 matrix-function (whose derivative is an integrable piecewise-continuous function) and $\boldsymbol{K}$ is a constant matrix. The determinant of $\boldsymbol{\Phi}$ is unity at $\tau = 2\pi$, $|\boldsymbol{\Phi}(2\pi)| = 1$ because

$$\operatorname{trace} \boldsymbol{D} = \sum_{j=1}^{4} D_{jj} = -4\varepsilon \frac{k_1 k_2}{k^2} = -\frac{1}{k^2} d_\tau k^2. \tag{2.30}$$

It follows that whenever λ is an eigenvalue of the monodromy matrix, $\boldsymbol{M} = \boldsymbol{\Phi}(2\pi)$, so too are its inverse λ^{-1} and its complex conjugate λ^* (see LZ04). Consequently, in the stable case, eigenvalues of $\boldsymbol{M}$ lie on the unit circle. If any eigenvalue λ of $\boldsymbol{M}$ has modulus exceeding one, this implies that there is indeed an exponentially growing solution. The growth rates are then given by

$$\sigma = \frac{1}{2\pi} \log(\lambda). \tag{2.31}$$

In the Floquet system (2.28) figure four dimensionless parameters, namely

$$\varepsilon = \tfrac{1}{2}\left(E - E^{-1}\right), \quad \mu = k_3/k_0, \quad \mathcal{N} = N/\Omega, \quad \mathcal{B} = (k_0 B)/\Omega, \tag{2.32a–d}$$

where $k_0 = \sqrt{k_p^2 + k_3^2}$ represents the modulus of the initial wave vector for $\varepsilon = 0$. The parameters $k_0 B$, N and 2Ω can be seen as the maximal frequencies of Alfvén, gravity and inertial waves, respectively (we return to this later).

For the stability analysis of system (2.28), we perform an asymptotic analysis to leading order in ε to determine the maximal growth rates of instability (if it exists). In addition, we integrate numerically (using the fourth-order Runge–Kutta–Gill method) system (2.28) from $\tau = 0$ to $\tau = 2\pi$ and we determine the eigenvalues of the solution matrix numerically (using the double QR method).

3. Destabilised resonances of MIG waves

In this section, we start from the case of a vertically stratified flow with (horizontal) circular streamlines subjected to a vertical magnetic field. In that case, there are

MIG waves. We characterise the resonant cases of these waves because some of them become destabilising when the streamlines are elliptical ($\varepsilon \neq 0$). We perform an asymptotic analysis to leading order in ε of the Floquet system (2.28) and determine the maximal growth rate of the destabilising resonant cases of order $n = 2$ (called subharmonic instability). The asymptotic analysis is performed by extending analytical techniques developed by LZ04. For the sake of clarity, all the asymptotic calculations are reported in Appendix A. Here we only state the results.

3.1. *Dispersion relation of MIG waves*

In this section, we establish the dispersion relation of the MIG waves propagating in a non-diffusive unbounded fluid. The cases of inertia-gravity waves and magneto-inertia waves are briefly addressed. We denote by $\boldsymbol{D}_0$ the matrix $\boldsymbol{D}$ for $E = 1$ (i.e. circular streamlines)

$$\boldsymbol{D}_0 = \Omega^{-1} \begin{pmatrix} 0 & -2\Omega & \mathrm{i}\omega_a & 0 \\ (2\Omega)^{-1}\omega_r^2 & 0 & 0 & \mathrm{i}\left(\omega_a^2 + \omega_g^2\right)\omega_a^{-1} \\ \mathrm{i}\omega_a & 0 & 0 & 0 \\ 0 & \mathrm{i}\omega_a & 0 & 0 \end{pmatrix}, \tag{3.1}$$

where

$$\omega_r = 2\boldsymbol{\Omega} \cdot (\boldsymbol{k}/k) = 2\Omega\mu, \tag{3.2a}$$

$$\omega_a = \boldsymbol{B} \cdot \boldsymbol{k} = Bk_0\mu = \Omega\mathcal{B}\mu, \tag{3.2b}$$

$$\omega_g = N|\boldsymbol{g} \times \boldsymbol{k}|/(gk) = N\sqrt{1-\mu^2} = \Omega\mathcal{N}\sqrt{1-\mu^2} \tag{3.2c}$$

are the frequencies of inertial, Alfvèn and gravity waves, respectively. The eigenvalues σ_j ($j = 1, 2, 3, 4$) of the constant matrix $\boldsymbol{D}_0$ take the form (Salhi *et al.* 2017),

$$-\Omega^2\sigma_{1,2}^2 = \omega_{1,2}^2 = \frac{1}{2}\left[2\omega_a^2 + \omega_r^2 + \omega_g^2 + \sqrt{\left(\omega_r^2 + \omega_g^2\right)^2 + 4\omega_r^2\omega_a^2}\right], \tag{3.3a}$$

$$-\Omega^2\sigma_{3,4}^2 = \omega_{3,4}^2 = \frac{1}{2}\left[2\omega_a^2 + \omega_r^2 + \omega_g^2 - \sqrt{\left(\omega_r^2 + \omega_g^2\right)^2 + 4\omega_r^2\omega_a^2}\right], \tag{3.3b}$$

or, equivalently,

$$\omega_1 = -\omega_2 = \frac{\Omega}{\sqrt{2}}\sqrt{\left(4 + 2\mathcal{B}^2 - \mathcal{N}^2\right)\mu^2 + \mathcal{N}^2 + \sqrt{\left[\left(4 - \mathcal{N}^2\right)\mu^2 + \mathcal{N}^2\right]^2 + 16\mathcal{B}^2\mu^4}}, \tag{3.4a}$$

$$\omega_3 = -\omega_4 = \frac{\Omega}{\sqrt{2}}\sqrt{\left(4 + 2\mathcal{B}^2 - \mathcal{N}^2\right)\mu^2 + \mathcal{N}^2 - \sqrt{\left[\left(4 - \mathcal{N}^2\right)\mu^2 + \mathcal{N}^2\right]^2 + 16\mathcal{B}^2\mu^4}}. \tag{3.4b}$$

These are distinct and non-zero as long as

$$\mathcal{B} \neq 0 \quad \text{and} \quad 0 < \mu^2 < 1. \tag{3.5}$$

In the non-stratified case ($\mathcal{N} = 0$), the frequencies $\omega_{1,2,3,4}$ are linear with respect to the variable μ (see (3.8)); in the presence of stratification, they are not. This has

the consequence of making the asymptotic analysis calculations much more complex (see Appendix A) than in the cases without stratification which were studied by LZ04 (the magneto-elliptical instability) and Mizerski & Bajer (2009) (the magneto-elliptical instability of rotating systems).

On the other hand, we note that (3.3), which can be rewritten as follows (Salhi *et al.* 2017)

$$\left(\omega^2 - \omega_g^2\right)\left(\omega^2 - \omega_a^2 - \omega_g^2\right) - \omega_r^2\omega^2 = 0, \tag{3.6}$$

represents the dispersion relation for MIG waves in a non-diffusive fluid. As it was discussed in Salhi *et al.* (2017), the dispersion relation (3.6) remains similar to that of f-plane MHD (Schecter, Boyd & Gilman 2001).

We can gain insight into the analysis of resonant cases of MIG waves by examining some limiting cases.

3.1.1. *Inertia-gravity waves*

In the absence of unperturbed magnetic field ($B = 0$, so that, $\omega_a = 0$), the frequency $\omega_{3,4}$ given by (3.3) vanishes, whereas the frequency $\omega_{1,2}$ reduces to

$$\omega_{1,2} = \pm\sqrt{\omega_g^2 + \omega_r^2} = \Omega\sqrt{(4 - \mathcal{N}^2)\mu^2 + \mathcal{N}^2}. \tag{3.7}$$

In that case, there are inertia-gravity waves where the simultaneous presence of the solid-body rotation and stable vertical stratification produces higher-frequency waves because $\omega_r^2 \leq \omega_{1,2}^2$ and $\omega_g^2 \leq \omega_{1,2}^2$.

3.1.2. *Magneto-inertia waves*

In the non-stratified case, $N = 0$, the frequency of gravity waves vanishes, $\omega_g = 0$. In that case, there are fast and slow magneto-inertia waves with frequency

$$\omega_{1,2} = \pm\tfrac{1}{2}\left(\sqrt{\omega_r^2 + 4\omega_a^2} + \omega_r\right) = \pm\Omega\left(\sqrt{1 + \mathcal{B}^2} + 1\right)\mu, \tag{3.8a}$$

$$\omega_{3,4} = \pm\tfrac{1}{2}\left(\sqrt{\omega_r^2 + 4\omega_a^2} - \omega_r\right) = \pm\Omega\left(\sqrt{1 + \mathcal{B}^2} - 1\right)\mu, \tag{3.8b}$$

respectively. Note that, in the study by LZ04, the fast magneto-inertia waves are called 'hydrodynamic modes' and the slow magneto-inertia waves are called 'magnetic modes' because $\omega_{3,4} = 0$ at vanishing unperturbed magnetic field.

3.2. *Resonant cases of MIG waves*

In this section, we establish the condition of resonances of order n between two fast or between two slow modes or between a fast mode and a slow mode.

The resonant cases of MIG waves are those parameter values $(\mu, \mathcal{N}, \mathcal{B},)$ such that

$$\omega_i - \omega_j = n\Omega, \quad (i \neq j), \tag{3.9}$$

where n is an integer. For the elliptical flow, the only resonant cases that can lead to instability are those for which the integer n is even.

By using (3.3) we deduce that the resonance condition between two fast modes ($\omega_1 - \omega_2 = n\Omega$) or between two slow modes ($\omega_3 - \omega_4 = n\Omega$) is described by the following algebraic equation,

$$4\mathcal{B}^2\left(\mathcal{B}^2 - \mathcal{N}^2\right)\mu^4 + \left(4\mathcal{B}^2\mathcal{N}^2 - 2n^2\mathcal{B}^2 - 4n^2 + n^2\mathcal{N}^2\right)\mu^2 + n^2\left(\frac{n^2}{4} - \mathcal{N}^2\right) = 0, \tag{3.10}$$

with $0 < \mu^2 < 1$. Because the replacement $\mu \to -\mu$ and/or $n \to -n$ in (3.10) result in the same condition, we may therefore assume without loss of generality that $\mu > 0$ and $n > 0$.

The condition (3.10) for resonance readily extends that by Bayly (1986) for basic elliptical flow instability ($\mathcal{B} = 0$ and $\mathcal{N} = 0$). Note that π/Ω is the typical time (period) for a wave packet to run the closed elliptical streamline, in the limit of vanishing, but non-zero, ε; in the same limit, this period characterises the periodic alignment of the fluctuating vorticity with the mean (weak) strain, as $2\pi/\omega$. The condition can be written $4\Omega\mu = n\Omega$ from the seminal study (Bayly 1986), that immediately yielded $\mu = n/4 = 0.5$ (because only $n = 2$ gives rise to $\mu < 1$), giving the origin of time-dependent instability tongues at vanishing ε. Even if a single-mode analysis is apparently sufficient, as emphasised by Craik & Criminale (1986) without the need for nonlinearity (exact solution), a two-mode resonance is implied, as also suggested by the classical normal mode analysis. For both basic elliptical flow instability and precessional instability, we have to consider the modes with dispersion law $\omega_1 = +\omega_r$ and $\omega_2 = -\omega_r$, and the subharmonic destabilising resonance is found for $\omega_1 - \omega_2 = 2\omega_r = \pm n\Omega$. Accordingly, the subharmonic order is $n = 2$ for the basic elliptical flow instability, and $n = 1$ for the precessional instability. Also in agreement with his *triad instability principle*, a detailed analysis of Waleffe (1992) shows that the elliptical instability corresponds to a forward (F)-interaction: the two modes with eigenfrequency ω_1 and ω_2 have opposite polarities and are coupled with the mean flow, which is associated to a zero frequency, the unstable modes are thereby two resonant inertial waves associated with the uniform background rotation.

In a similar manner, we determine from (3.3) the resonance condition between a fast mode and a slow mode ($\omega_1 - \omega_3 = n\Omega$ or $\omega_1 - \omega_4 = n\Omega$),

$$\left[\left(4 - \mathcal{N}^2\right)^2 + 16\mathcal{B}^2\right]\mu^4 - 2\left[2n^2\mathcal{B}^2 + \left(\mathcal{N}^2 - 4\right)\left(\mathcal{N}^2 - n^2\right)\right]\mu^2 + \left(\mathcal{N}^2 - n^2\right)^2 = 0. \tag{3.11}$$

In the three following sections, we present asymptotic formulae for the maximal growth rates of the subharmonic instabilities (those corresponding to the destabilising resonances of order $n = 2$). The asymptotic formulae are yielded by the asymptotic analysis at leading order in ε of the Floquet system (2.28). Obviously, the instabilities related to higher-order resonances ($n = 4, 6, 8, \ldots$) are excluded by the procedure leading to the asymptotic formulae. These instabilities (if they exist) can be captured by the numerical computations (see § 4).

3.3. *Destabilising resonance between two fast modes*

As shown by LZ04, the universal elliptic instability, which results from the resonances (of order $n = 2$) between two fast modes, persists in the presence of magnetic fields of arbitrary strength, although the growth rate decreases somewhat (LZ04). As a counterpart,

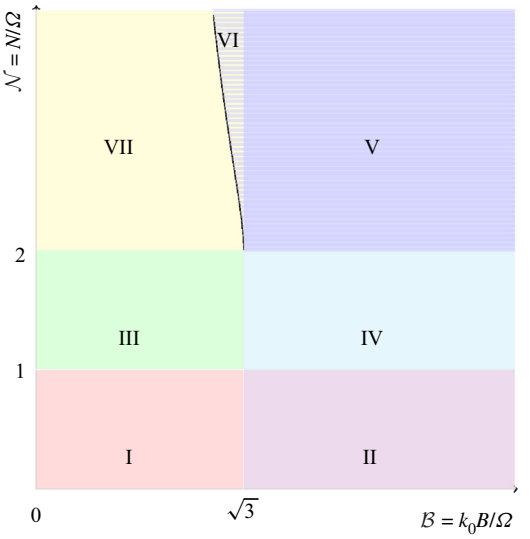

Figure 2. Domains of the $(\mathcal{B}, \mathcal{N})$ plane for which the magneto-gravity-elliptic instability operates. The subharmonic instability resulting from a resonance (of order $n = 2$) between two fast modes (referred to as IF instability) exists for $(\mathcal{B}, \mathcal{N})$ belonging to domains I, II and VI. The subharmonic instability resulting from a resonance between two slow modes (referred to as IS instability) exists for $(\mathcal{B}, \mathcal{N})$ belonging to domains II, IV, V and VI. The subharmonic instability resulting from a resonance between a fast mode and a slow mode (referred to as IM instability) exists for $(\mathcal{B}, \mathcal{N})$ belonging to domains I, II, III and IV. For $(\mathcal{B}, \mathcal{N})$ belonging to domain VII, there is no subharmonic instability, whereas instabilities related to higher order resonances ($n = 4, 6, 8, \ldots$) can exist. Domain I: $(\mathcal{B}, \mathcal{N}) \in [0, \sqrt{3}] \times [0, 1]$; domain II: $(\mathcal{B}, \mathcal{N}) \in [\sqrt{3}, +\infty[\times [0, 1]$; domain III: $(\mathcal{B}, \mathcal{N}) \in [0, \sqrt{3}] \times [1, 2]$; domain IV: $(\mathcal{B}, \mathcal{N}) \in [\sqrt{3}, +\infty[\times [1, 2]$; domain V: $(\mathcal{B}, \mathcal{N}) \in [\sqrt{3}, +\infty[\times [2, +\infty[$; domain VI: $(\mathcal{B}, \mathcal{N}) \in \mathcal{D}_f$ where $\mathcal{D}_f$ is defined by (3.13); domain VII: $(\mathcal{B}, \mathcal{N}) \in [0, \sqrt{3}[\times [2, +\infty[\backslash \mathcal{D}_f$.

in the presence of vertical (stable) stratification, it is completely suppressed when $\mathcal{N}$ reaches 1 (Miyazaki & Fukumoto 1992). In this section, we investigate the effects of the axial (stable) stratification and magnetic field when there are simultaneously present on this instability (referred to as IF instability).

A detailed analysis of the algebraic equation (3.10), knowing that $0 \leq \mu^2 \leq 1$, $0 \leq \mathcal{B} < +\infty$ and $0 \leq \mathcal{N} < +\infty$, indicates that the resonant case of order $n = 2$ between two fast modes ($\omega_1 - \omega_2 = 2\Omega$) exists for

$$(\mathcal{B}, \mathcal{N}) \in ([0, +\infty[\times [0, 1]) \cup \mathcal{D}_f, \tag{3.12}$$

which corresponds to the domains I, II and VI of the plane $(\mathcal{B}, \mathcal{N})$ shown by figure 2. Here, the domain $\mathcal{D}_f$ is defined as follows:

$$\forall\, (\mathcal{B}, \mathcal{N}) \in \mathcal{D}_f \Leftrightarrow \text{ for given } \mathcal{N} \in]2, +\infty[\quad \Longrightarrow \quad 1 < f(\mathcal{N}) \leq \mathcal{B} < \sqrt{3}, \tag{3.13}$$

where $f :]2, +\infty[\to]1, \sqrt{3}[$ is a continuous decreasing function with reciprocal function $f^{-1} :]1, \sqrt{3}[\to]2, +\infty[$,

$$\forall \mathcal{N} \in]2, +\infty[,\ f(\mathcal{N}) = \frac{1}{\mathcal{N}^2}\sqrt{\mathcal{N}^4 + 4\mathcal{N}^2 - 8 + 4\sqrt{(\mathcal{N}^2 - 1)(\mathcal{N}^4 - 4)}} \underset{\mathcal{N} \to +\infty}{\longrightarrow} 1, \tag{3.14a}$$

$$\forall \mathcal{B} \in]1, \sqrt{3}[,\ f^{-1}(\mathcal{B}) = \frac{2}{(\mathcal{B}^2 - 1)}\sqrt{1 + \mathcal{B}^2 + \mathcal{B}\sqrt{4 - (\mathcal{B}^2 - 1)^2}} \underset{\mathcal{B} \to 1^+}{\longrightarrow} +\infty. \tag{3.14b}$$

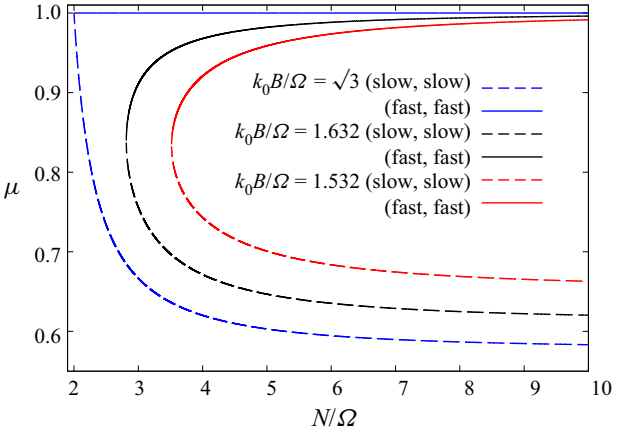

Figure 3. Resonant cases of order $n = 2$ in the case where $(\mathcal{B}, \mathcal{N}) \in \mathcal{D}_f$ (see (3.13)). Variation of $\mu = \cos(\theta) = k_3/k_0$ versus $\mathcal{N} = N/\Omega$ for $\mathcal{B} = k_0 B/\Omega = \sqrt{3}$, 1.632 and $\mathcal{B} = 1.532$. Solid lines represent the resonances between two fast modes (fast, fast) and dotted lines represent the resonances between two slow modes (slow, slow).

For $(\mathcal{B}, \mathcal{N})$ belonging to the domain given by (3.12), the resonances (of order $n = 2$) between two fast modes occur when

$$\mu^2 = \frac{1 - \mathcal{N}^2}{4 - \mathcal{N}^2} \quad \text{if } \mathcal{B} = 0, \tag{3.15a}$$

$$\mu^2 = \frac{\mathcal{B}^2 - 1}{\mathcal{B}^4 - \mathcal{B}^2 - 4} \quad \text{if } \mathcal{B} = \mathcal{N}, \tag{3.15b}$$

$$\mu^2 = \frac{(1 + \mathcal{B}^2)(1 - \mathcal{N}^2) + \mathcal{B}^2 + 3 - \sqrt{\Delta}}{2\mathcal{B}^2(\mathcal{B}^2 - \mathcal{N}^2)} \quad \text{if } \mathcal{B} \neq \mathcal{N}, \tag{3.15c}$$

where

$$\Delta(\mathcal{B}, \mathcal{N}) = \left(\mathcal{N}^2\left(\mathcal{B}^2 - 1\right) - 4\right)^2 + 16\left(\mathcal{B}^2 - \mathcal{N}^2\right). \tag{3.16}$$

It immediately follows that

$$\lim_{0 \leq \mathcal{N} \leq 1, \mathcal{B} \to +\infty} \mathcal{B}^2\mu^2 = 1 - \mathcal{N}^2, \qquad \lim_{1 < \mathcal{B} < \sqrt{3}, \mathcal{N} \to +\infty} \mathcal{B}^2\mu^2 = 1. \tag{3.17a,b}$$

In the non-stratified magnetised case ($\mathcal{N} = 0$), the parameter $\mu = [1 + \sqrt{1 + \mathcal{B}^2}]^{-1}$ changes from 0.5 (so that, $\theta = \widehat{(\boldsymbol{k}, \boldsymbol{W})} = \cos^{-1}(\mu) = \pi/3$) at $\mathcal{B} = 0$ to zero (so that, $\theta = \pi/2$) as $\mathcal{B} \to +\infty$ (see also LZ04). Recall that $\boldsymbol{k}$ denotes the wave vector and $\boldsymbol{W} = \boldsymbol{\nabla} \times \boldsymbol{U}$ denotes the basic vorticity vector. In the non-magnetised stratified case ($\mathcal{B} = 0$), the parameter $\mu = \sqrt{(1 - \mathcal{N}^2)/(4 - \mathcal{N}^2)}$ changes from $\mu = 0.5$ at $\mathcal{N} = 0$ to $\mu = 0$ at $\mathcal{N} = 1$. For $(\mathcal{B}, \mathcal{N}) \in [0, +\infty[\times [0, 1]$ and when $\mathcal{B}$ is fixed, the parameter μ changes from $\mu = [1 + \sqrt{1 + \mathcal{B}^2}]^{-1}$ at $\mathcal{N} = 0$ to $\mu = 0$ at $\mathcal{N} = 1$. For $(\mathcal{B}, \mathcal{N}) \in \mathcal{D}_f$ and when $\mathcal{B}$ is fixed, the parameter μ increases from $\mu(\mathcal{B}, f(\mathcal{B}))$ at $\mathcal{N} = f(\mathcal{B})$ to $\mu = 1$ as $\mathcal{N} \to +\infty$. As an illustration, figure 3 shows the variation of μ versus $\mathcal{N}$ for three values of $\mathcal{B} = \sqrt{3}$, 1.632 and 1.532.

According to our asymptotic analysis at leading order in ε (see Appendix A), the maximal growth rate of the subharmonic instability (if it exists) resulting from the resonance between two fast modes is of the form

$$\frac{\sigma_{mf}}{\varepsilon} = \frac{\left(3-\mathcal{B}^2\mu^2\right)\left(1+\mathcal{B}^2\mu^2\right)}{8}\frac{\left[\left(\mathcal{N}^2-\mathcal{B}^2+2\right)\mu^2+\left(1-\mathcal{N}^2\right)\right]}{\left[\left(\mathcal{N}^2-2\mathcal{B}^2-4\right)\mu^2+\left(2-\mathcal{N}^2\right)\right]} \tag{3.18}$$

in which μ^2 is given by (3.15).

Some results reported in previous studies (Waleffe 1990; Kerswell 2002 and LZ04) can be recovered from (3.18) by using (3.15)

$$\frac{\sigma_{mf}}{\varepsilon} = \frac{9}{16} \quad \text{for } \mathcal{N}=0,\ \mathcal{B}=0, \tag{3.19a}$$

$$\frac{\sigma_{mf}}{\varepsilon} = \frac{9}{4}\frac{(1-\mathcal{N}^2)}{(4-\mathcal{N}^2)} \quad \text{for } 0\le\mathcal{N}\le 1,\ \mathcal{B}=0, \tag{3.19b}$$

$$\frac{\sigma_{mf}}{\varepsilon} = \frac{1}{4}\left(1+\frac{1}{\sqrt{\mathcal{B}^2+1}+1}\right)^2 \quad \text{for } \mathcal{N}=0,\ 0\le\mathcal{B}<+\infty. \tag{3.19c}$$

Equation (3.19*b*) indicates that the maximal growth rate is zero at $\mathcal{N}=1$. Therefore, in the non-magnetised stratified case ($\mathcal{B}=0$), the subharmonic instability is completely suppressed by stratification when $\mathcal{N}$ reaches 1 (Miyazaki & Fukumoto 1992; Kerswell 2002). For the non-stratified magnetised case ($\mathcal{N}=0$), (3.19*c*) indicates that σ_{mf}/ε decreases as $\mathcal{B}$ increases so as (see also LZ04)

$$\lim_{\mathcal{N}=0,\ \mathcal{B}\to+\infty}\frac{\sigma_{mf}}{\varepsilon} = \frac{1}{4}. \tag{3.20}$$

However, in the stratified magnetised case, the analysis of (3.18) is more subtle as shown in the following.

For $(\mathcal{B},\mathcal{N})\in\,]0,+\infty[\,\times\,]0,1]$ and when $\mathcal{N}$ is fixed, σ_{mf}/ε also decreases from $\sigma_{mf}/\varepsilon=[9(1-\mathcal{N}^2)]/[4(4-\mathcal{N}^2)]$ at $\mathcal{B}=0$ to zero (and not to 1/4) as $\mathcal{B}\to+\infty$. Indeed, from (3.18), one easily deduces that

$$\lim_{0<\mathcal{N}\le 1,\ \mathcal{B}\to+\infty}\frac{\sigma_{mf}}{\varepsilon} = 0, \tag{3.21}$$

because $\lim_{\mathcal{B}\to+\infty}\mathcal{B}^2\mu^2 = 1-\mathcal{N}^2$, as indicated previously. Therefore, the $\mathcal{N}\to 0$ limit is, in fact, singular (discontinuous). As an illustration, figure 4 shows σ_{mf}/ε versus $\mathcal{B}$ for five values of $\mathcal{N}=0.0,\,0.2,\,0.5,\,0.7$ and 0.9. At $\mathcal{N}=1$, one has $\sigma_{mf}=0$ independently of $\mathcal{B}$.

For $(\mathcal{B},\mathcal{N})\in\mathcal{D}_f$ and for fixed $\mathcal{N}$, the maximal growth rate σ_{mf} increases from 0 at $\mathcal{B}=\sqrt{3}$ to $\sigma_{mf}(f(\mathcal{N}),N)$ at $\mathcal{B}=f(\mathcal{N})$ with

$$\lim_{\mathcal{N}\to+\infty}\frac{\sigma_{fm}\left(f\left(\mathcal{N}\right),N\right)}{\varepsilon} = \frac{1}{2}. \tag{3.22}$$

This is illustrated by figure 5 which displays the variation of σ_{mf}/ε versus $\mathcal{B}\,(1<\mathcal{B}<\sqrt{3})$ for $\mathcal{N}=10$ and $\mathcal{N}=50$. Therefore, this subharmonic instability, which occurs when

$$2\Omega < N < +\infty \quad \text{and} \quad \Omega < k_0 B = \Omega f(\mathcal{N}) < \sqrt{3}\,\Omega, \tag{3.23a,b}$$

is the results of the simultaneous presence of axial (stable) stratification and magnetic field. On the other hand, the above analysis clearly shows that, for $(\mathcal{B},\mathcal{N})\in[0,+\infty[\,\times\,[0,1]$,

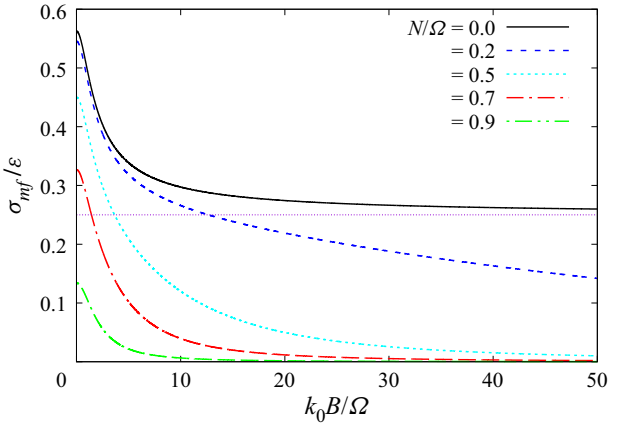

Figure 4. Maximal growth rate of the destabilising resonances of order n = 2 between two fast modes (see (3.18)). The figure shows σ_{mf}/ε vs $\mathcal{B} = k_0 B/\Omega$ for $\mathcal{N} = N/\Omega = 0$, 0.2, 0.5, 0.7 and $\mathcal{N} = 0.9$.

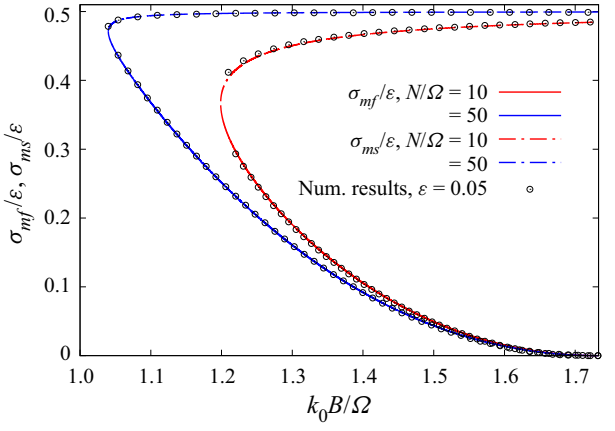

Figure 5. Maximal growth rates of subharmonic instabilities resulting from the resonances between two fast modes (σ_{mf}) or between two slow modes (σ_{ms}) in the case where $(\mathcal{B}, \mathcal{N}) \in \mathcal{D}_f$ (see (3.13)). The variation of σ_{mf}/ε and σ_{ms}/ε versus $\mathcal{B} = k_0 B/\Omega$ for $\mathcal{N} = N/\Omega = 10$ and $\mathcal{N} = 50$ is shown. Numerical results (see § 4) for $\varepsilon = 0.05$ are represent by symbols.

the IF instability is completely suppressed by the stratification when $\mathcal{N}$ reaches 1. When $0 < \mathcal{N} < 1$, stratification acts to render the IF instability less efficient especially for large $\mathcal{B}$ because its maximal growth approaches zero as $\mathcal{B} \to +\infty$ (see (3.21)).

3.4. *Destabilising resonances between two slow modes*

As shown by LZ04, in the presence only of the magnetic field, there exist other subharmonic instabilities, which are due to the presence of the magnetic field, in addition to the universal elliptical instability. One of them is the subharmonic instability resulting from the resonances (of order $n = 2$) between two slow modes (referred to as IS instability). In this section, we study the effects of the vertical (stable) stratification on the IS instability.

From the resonant condition described by relation (3.10), we deduce that the resonant cases of order $n = 2$ between two slow modes, so that $\omega_3 - \omega_4 = 2\Omega$, exist for

$$(\mathcal{B}, \mathcal{N}) \in \left([\sqrt{3}, +\infty[\times [0, +\infty[\right) \cup \mathcal{D}_f. \tag{3.24}$$

This corresponds to the domains II, IV, V and VI shown in figure 2.

For $(\mathcal{B}, \mathcal{N})$ belonging to these domains, the resonant cases of order $n = 2$ between two slow modes occur at the following points of the μ axis

$$\mu^2 = \frac{\mathcal{B}^2 - 1}{\mathcal{B}^4 - \mathcal{B}^2 - 4} \quad \text{if } \mathcal{B} = \mathcal{N}, \tag{3.25a}$$

$$\mu^2 = \frac{(1 + \mathcal{B}^2)(1 - \mathcal{N}^2) + \mathcal{B}^2 + 3 + \sqrt{\Delta}}{2\mathcal{B}^2(\mathcal{B}^2 - \mathcal{N}^2)} \quad \text{if } \mathcal{B} \neq \mathcal{N}. \tag{3.25b}$$

It immediately follows that

$$\lim_{\mathcal{N} \geq 0,\ \mathcal{B} \to +\infty} \mu^2 \mathcal{B}^2 = 1, \qquad \lim_{\mathcal{B} > 1,\ \mathcal{N} \to +\infty} \mu^2 \mathcal{B}^2 = 1. \tag{3.26a,b}$$

In the non-stratified magnetised case, (3.25) reduces to $\mu = [\sqrt{\mathcal{B}^2 + 1} - 1]^{-1}$, or equivalently, $\mu^2 \mathcal{B}^2 = 1 + 2\mu$. Thus, the parameter μ changes from 1 at $\mathcal{B} = \sqrt{3}$ to 0 as $\mathcal{B} \to +\infty$ (see also LZ04). In the stratified magnetised case, (3.25) indicates that, at fixed $\mathcal{B}$ such that $(\mathcal{B}, \mathcal{N}) \in [\sqrt{3}, +\infty[\times [0, +\infty[$, the parameter μ changes from $\mu = [\sqrt{\mathcal{B}^2 + 1} - 1]^{-1}$ at $\mathcal{N} = 0$ to $\mu = 1/\mathcal{B}$ as $\mathcal{N} \to +\infty$. For fixed $\mathcal{B}$ such that $(\mathcal{B}, \mathcal{N}) \in \mathcal{D}_f$, the parameter μ decreases from $\mu(\mathcal{B}, f(\mathcal{B}))$ at $\mathcal{N} = f(\mathcal{B})$ to $\mu = 1/\mathcal{B}$ as $\mathcal{N} \to +\infty$ (see figure 3).

As shown in Appendix A, the maximal growth rate, denoted by σ_{ms}, of the IS instability is also described by (3.18) (repeated here for the sake of clarity)

$$\frac{\sigma_{ms}}{\varepsilon} = \frac{\left(3 - \mathcal{B}^2\mu^2\right)\left(1 + \mathcal{B}^2\mu^2\right)}{8} \frac{\left[\left(\mathcal{N}^2 - \mathcal{B}^2 + 2\right)\mu^2 + \left(1 - \mathcal{N}^2\right)\right]}{\left[\left(\mathcal{N}^2 - 2\mathcal{B}^2 - 4\right)\mu^2 + \left(2 - \mathcal{N}^2\right)\right]} \tag{3.27}$$

in which μ is now given by (3.25) and not by (3.15).

In the non-stratified magnetised case ($\mathcal{N} = 0$), (3.27) reduces to

$$\frac{\sigma_{ms}}{\varepsilon} = \frac{1}{4}\left(1 - \frac{1}{\sqrt{\mathcal{B}^2 + 1} - 1}\right)^2 \underset{\mathcal{N}=0,\ \mathcal{B} \to +\infty}{\longrightarrow} \frac{1}{4}, \tag{3.28}$$

where $\sqrt{3} < \mathcal{B} < +\infty$, in agreement with the previous results by LZ04. In that case, σ_{ms}/ε increases from 0 at $\mathcal{B} = \sqrt{3}$ to 1/4 as $\mathcal{B} \to +\infty$.

For $(\mathcal{B}, \mathcal{N}) \in ([\sqrt{3}, +\infty[\times [0, +\infty[) \cup \mathcal{D}_f$, we use (3.26a,b) to deduce from (3.27) the following limits

$$\lim_{\mathcal{N} > 0,\ \mathcal{B} \to +\infty} \frac{\sigma_{ms}}{\varepsilon} = \frac{1}{2}, \qquad \lim_{\mathcal{B} > 1,\ \mathcal{N} \to +\infty} \frac{\sigma_{ms}}{\varepsilon} = \frac{1}{2}. \tag{3.29a,b}$$

Indeed, when $\mathcal{B} \gg 1$ and $\mathcal{B} \gg \mathcal{N} > 0$, an equivalent form for σ_{ms}/ε can be written as

$$\frac{\sigma_{ms}}{\varepsilon} \underset{\mathcal{B} \to +\infty}{\sim} \frac{\left(3 - \mathcal{B}^2\mu^2\right)\left(1 + \mathcal{B}^2\mu^2\right)}{8} \frac{\left(1 - \mathcal{N}^2 - \mathcal{B}^2\mu^2\right)}{\left(2 - \mathcal{N}^2 - 2\mathcal{B}^2\mu^2\right)} \underset{\mathcal{B} \to +\infty}{\longrightarrow} \frac{1}{2} \tag{3.30}$$

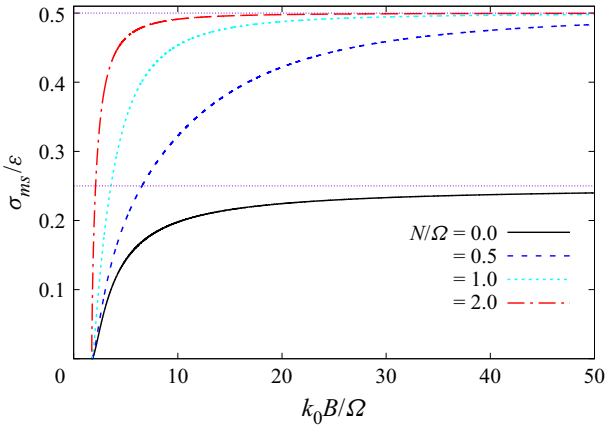

Figure 6. Maximal growth rate of the destabilising resonances of order $n = 2$ between two slow modes (see (3.27)). The figure shows σ_{ms}/ε versus $\mathcal{B}$ for $\mathcal{N} = 0.0$, 0.5, 1.0, 2 and $\mathcal{N} = 3$.

because $\lim_{\mathcal{B}\to+\infty} \mu^2\mathcal{B}^2 = 1$. When $\mathcal{N} \gg \mathcal{B} > 1$, an equivalent form for σ_{ms}/ε can be written as

$$\frac{\sigma_{ms}}{\varepsilon} \underset{\mathcal{N}\to+\infty}{\sim} \frac{\left(3-\mathcal{B}^2\mu^2\right)\left(1+\mathcal{B}^2\mu^2\right)}{8} \underset{\mathcal{N}\to+\infty}{\longrightarrow} \frac{1}{2} \tag{3.31}$$

because $\lim_{\mathcal{N}\to+\infty} \mu^2\mathcal{B}^2 = 1$.

It follows that, for $(\mathcal{B},\mathcal{N}) \in [\sqrt{3}, +\infty[\times [0, +2]$ and when $\mathcal{N}$ is fixed, σ_{ms}/ε increases from 0 at $\mathcal{B} = \sqrt{3}$ to 0.5 as $\mathcal{B} \to +\infty$. This is illustrated by figure 6 which shows σ_{ms}/ε versus $\mathcal{B}$ for $\mathcal{N} = 0$, 0.5, 1 and $\mathcal{N} = 2$. By comparing (3.28) and (3.31), we can remark that, in this case, the $\mathcal{N} \to 0$ limit is, in fact, singular (discontinuous). Consequently, we can conclude that in the presence of the stratification with $\mathcal{N} \leq 2$ the IS instability is reinforced because σ_{ms}/ε tends towards $1/2$ like $\mathcal{B} \to +\infty$, whereas without stratification ($\mathcal{N} = 0$), σ_{ms}/ε approaches $1/4$.

On the other hand, for $(\mathcal{B},\mathcal{N}) \in \mathcal{D}_f \cup ([\sqrt{3}, +\infty[\times]2, +\infty[)$ (this corresponds to the domains V and VI shown in figure 2) and when $\mathcal{N}$ is fixed, σ_{ms}/ε also increases from $\sigma_{mf}(f(\mathcal{N}),\mathcal{N})/\varepsilon$ at $\mathcal{B} = f(\mathcal{N})$ to 0.5 as $\mathcal{B} \to +\infty$. Indeed, for $(\mathcal{B}_1,\mathcal{N}) \in \mathcal{D}_f$ and $(\mathcal{B}_2,\mathcal{N}) \in [\sqrt{3}, +\infty[\times]2, +\infty[$, we have (see figure 5),

$$0 \leq \sigma_{mf}(\mathcal{B}_1,\mathcal{N}) \leq \sigma_{ms}(\mathcal{B}_1,\mathcal{N}) \leq \sigma_{ms}(\mathcal{B}_2,\mathcal{N}) < \frac{\varepsilon}{2}. \tag{3.32}$$

It clearly appears that in the simultaneous presence of the axial magnetic field and stratification with $\mathcal{N} > 2$, the subharmonic instability resulting from the resonances (of order $n = 2$) between two slow modes, which emerges beyond the threshold $\mathcal{B}_c = f(\mathcal{N}) < \sqrt{3}$, is dominant with a maximal growth rate approaching $\varepsilon/2$ for large $\mathcal{B}$.

3.5. *Destabilising resonances between a fast mode and a slow mode*

In this section, we study the effects of the vertical (stable) stratification on the subharmonic instability resulting from the resonances (of order $n = 2$) between a fast mode and a slow mode (hereinafter, referred to as IM instability). Without stratification, the IM instability occurs for all magnetic field strengths where its maximal growth rate approaches $\varepsilon/4$ as $\mathcal{B} \to +\infty$ (see LZ04).

The resonance of order $n = 2$ between a fast mode and a slow mode, i.e. $\omega_1 - \omega_3 = 2\Omega$ or $\omega_1 - \omega_4 = 2\Omega$, exists for

$$(\mathcal{B}, \mathcal{N}) \in]0, +\infty[\times [0, +\infty[. \tag{3.33}$$

In the case where $\omega_1 - \omega_4 = 2\Omega$, one has $\mu = 1$, but this resonant case does not induce any instability because the Floquet system (2.28) is stable at $\mu = 1$, as already indicated.

In the case where $\omega_1 - \omega_3 = 2\Omega$, we deduce from the algebraic equation (3.11) that the points of the $\mu-$axis characterising the resonances between a fast mode and a slow mode are given by

$$\mu^2 = \frac{\left(4 - \mathcal{N}^2\right)^2}{\left(4 - \mathcal{N}^2\right)^2 + 16\mathcal{B}^2}. \tag{3.34}$$

The latter expression implies that, for fixed $\mathcal{N} \geq 0$, the parameter μ decreases from 1 at $\mathcal{B} = 0$ to zero as $\mathcal{B} \to +\infty$. Inversely, for fixed $\mathcal{B} > 0$, the parameter μ increases from $\mu = 1/\sqrt{1 + \mathcal{B}^2}$ at $\mathcal{N} = 0$ to 1 as $\mathcal{N} \to +\infty$.

However, according to our asymptotic analysis (see Appendix A), only the resonant cases for which the couple $(\mathcal{B}, \mathcal{N})$ belongs to the domain $]0, +\infty[\times [0, 2[$ (this corresponds to the domains I–IV shown in figure 2), are destabilising. In that case, the maximal growth rate of the IM instability, denoted by σ_{mm}, is found as (see Appendix A.3.3)

$$\frac{\sigma_{mm}}{\varepsilon} = \frac{(1 - \mu^2)}{16} \frac{\left[(1 - \mu^2)(4 - \mathcal{N}^2) + 4\mathcal{N}^2\right]}{\sqrt{4 + \mathcal{N}^2}} \sqrt{\frac{(4 - \mathcal{N}^2)^3}{(4 - \mathcal{N}^2)^2 + \mathcal{B}^2\mathcal{N}^4}}. \tag{3.35}$$

It immediately follows that $\sigma_{mm} = 0$ for $\mathcal{N} = 2$, independently of the magnetic field strength.

In the non-stratified case ($\mathcal{N} = 0$), (3.35) reduces to

$$\frac{\sigma_{mm}}{\varepsilon} = \frac{1}{4}\left(1 - \mu^2\right)^2 = \frac{\mathcal{B}^4}{4\left(1 + \mathcal{B}^2\right)^2} \underset{\mathcal{B} \to +\infty}{\longrightarrow} \frac{1}{4}, \tag{3.36}$$

in agreement with the study by LZ04. Therefore, σ_{mm}/ε increases from 0 at $\mathcal{B} = 0$ to approach $1/4$ as $\mathcal{B} \to +\infty$.

However, in the simultaneous presence of the vertical (stable) stratification and the magnetic field and for fixed $\mathcal{N} \leq 2$, σ_{mm}/ε increases from 0 to reach its maximum value (which is less than $1/4$), then it decreases tending towards zero when $\mathcal{B} \to +\infty$. Also in this case, the $\mathcal{N} \to 0$ limit is, in fact, singular (discontinuous). As an illustration, figure 7 shows σ_{mm}/ε vs $\mathcal{B}$ for $\mathcal{N} = 0$, 0.5, 1, 1.5 and $\mathcal{N} = 2$.

We can therefore conclude that the effect of (stable) stratification on the IM instability is to suppress it if $\mathcal{N}$ exceeds 2, or to make it less efficient otherwise ($0 < \mathcal{N} < 2$) because σ_{mm} approaches zero for large $\mathcal{B}$.

4. Numerical results

In this section, we numerically determine the maximal growth rate of the dominant instability for a given value of the triplet $(\mathcal{B}, \mathcal{N}, \varepsilon)$ such that $0 \leq \mathcal{B} = B/\Omega \leq 4$ and $0 \leq \mathcal{N} = N/\Omega \leq 4$ and $0 \leq \varepsilon \leq 1$ (or, equivalently, $1 \leq E = \varepsilon + \sqrt{1 + \varepsilon^2} = 1 + \sqrt{2}$). We use the resonance conditions (3.10) and (3.11) for the identification of the instability (if it exists) and we compare the asymptotic formulae with the numerical results. At the end of this section, we briefly examine the effect of fluid diffusivity in a special case where the diffusion coefficients are equal ($\nu = \kappa = \eta$).

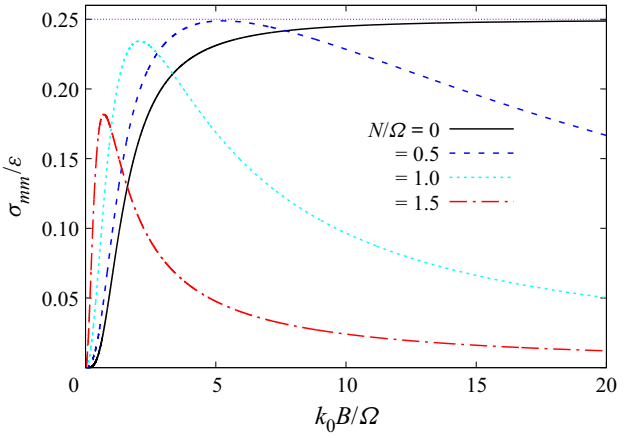

Figure 7. Maximal growth rate of the destabilising resonances of order $n = 2$ between a fast and a slow mode (see (3.35)). The figure shows σ_{mm}/ε versus $\mathcal{B}$ for $\mathcal{N} = 0.0, 0.5, 1.0$ and $\mathcal{N} = 1.5$.

4.1. *Identification of instabilities*

For the identification of the instabilities picked up by the numerical procedure we use the resonance conditions described by (3.10) and (3.11) as explained as follows.

On the one hand, for a given value of the couple $(\mathcal{B}, \mathcal{N})$, we use (3.15), (3.25) and (3.34) and determine the values of μ, say μ_0, characterising the resonant cases of order $n = 2$. On the other hand, for the same value of the couple $(\mathcal{B}, \mathcal{N})$, we consider several values of ε uniformly distributed in the interval $[0, 1]$ and, for each of these values of ε, we integrate numerically the Floquet system (2.28) and determine the growth rate σ for 2000 values of μ (evenly distributed) in $]0, 1[$. Obviously, $\sigma(\mu) = 0$ if there is no instability. Thus, in the plane $(\mu, \sigma + \varepsilon)$, the region of instability that emanates from the point of abscissa μ_0 characterises a subharmonic instability. As an illustration, figure 8 shows $\sigma + \varepsilon$ versus μ for $\mathcal{B} = 4$ and $\mathcal{N} = 0.5$ and 100 values of ε evenly distributed in the interval $[0, 0.8]$. In that case, there are three subharmonic instabilities IF, IM and IS which correspond to the regions of instability emanating from the points $(\mu_0 = 0.1755, 0)$, $(\mu_0 = 0.2282, 0)$ and $(\mu_0 = 3074, 0)$, respectively. The other instabilities appearing in figure 5 are related to higher-order resonances $(n = 4, 6, 8, \ldots)$, but as they are dominated by the subharmonic instabilities, we do not seek to identify them one by one.

4.2. *Comparison between the asymptotic formulae and the numerical results*

We recall that the present asymptotic results (at leading order in ε) clearly shows that subharmonic instability exists when

$$(\mathcal{B}, \mathcal{N}) \in ([0, +\infty[\times [0, 2]) \cup ([\sqrt{3} + \infty[\times [2, +\infty[) \cup \mathcal{D}_f. \tag{4.1}$$

Obviously, the procedure leading to the asymptotic formulae excludes the instabilities related to higher-order resonances $(n = 4, 6, 8, \ldots)$. Numerical calculations indicate that, when $(\mathcal{B}, \mathcal{N})$ belongs to domains I–VI (see figure 2) deprived of a very narrow band which are specified below, one of the subharmonic instabilities listed in § 3 is dominant.

In figure 9, we show the continuous variation of the maximal growth rate σ_m (maximum σ over $0 \leq \mu \leq 1$) of the dominant instability normalised by $\sigma_0 = 9/16$ plotted as a function of $0 \leq \mathcal{B} \leq 4$ and $0 \leq \mathcal{N} \leq 4$. Figure 9(*a*) displays the numerical results for

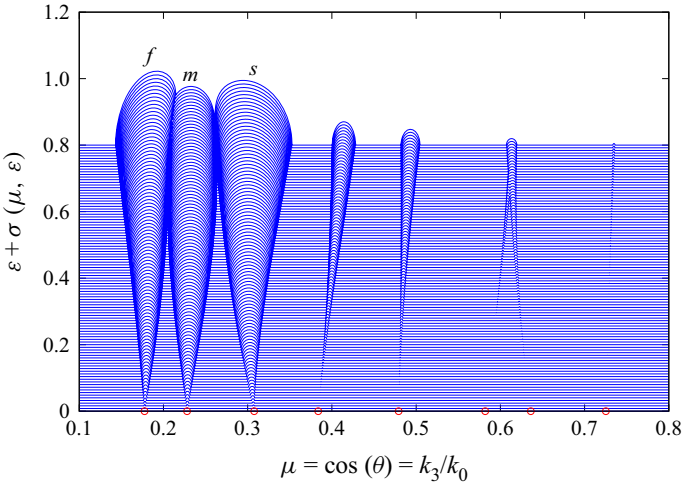

Figure 8. Magneto-gravity elliptic instabilities. The figure shows $\sigma + \varepsilon$ versus μ for $\mathcal{B} = 4$ and $\mathcal{N} = 0.5$ and 100 values of ε evenly distributed in the interval $[0, 0.8]$. The regions of instability labelled by f, m and s denote the IF, IM and IS instabilities that emanate from the points of the μ-axis of abscissa 0.1775, 0.2282 and 0.3074, respectively. The other instabilities picked up by the numerical procedure are related to higher-order resonances ($n = 4, 6, 8, \ldots$): for $n = 4$, $\mu = 0.3836$ (fast, fast), $\mu = 0.4792$ (fast, slow), $\mu = 0.6359$ (slow, slow); for $n = 6$, $\mu = 0.5821$ (fast, fast), $\mu = 0.7252$ (fast, slow).

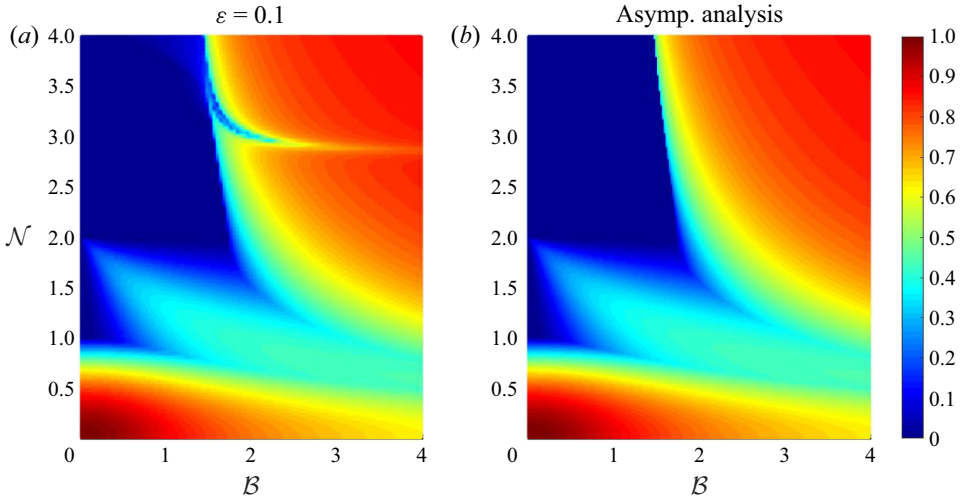

Figure 9. Magneto-gravity elliptic instabilities. Maximal growth rate of dominant instability normalised by $\sigma_0 = 9/16$ plotted as a function of $0 \le \mathcal{B} \le 4$ and $0 \le \mathcal{N} \le 4$.: (a) numerical results for $\varepsilon = 0.1$; (b) asymptotic analysis results.

$\varepsilon = 0.1$, where the grid consists of 201 points evenly distributed in each one of the ranges $0 \le \mathcal{B} \le 4$ and $0 \le \mathcal{N} \le 4$. Figure 9(a) shows the analytical results for σ_m/σ_0 where

$$\sigma_m = \max(\sigma_{mf}, \sigma_{ms}, \sigma_{mm}). \tag{4.2}$$

Recall that σ_{mf}, σ_{ms} and σ_{mm} are given by equations (3.18), (3.27) and (3.35), respectively.

As can be seen, the agreement between the numerical results and the asymptotic formulae is quite good except for $(\mathcal{B}, \mathcal{N})$ belonging to a narrow band around $\mathcal{N} = 3$ and

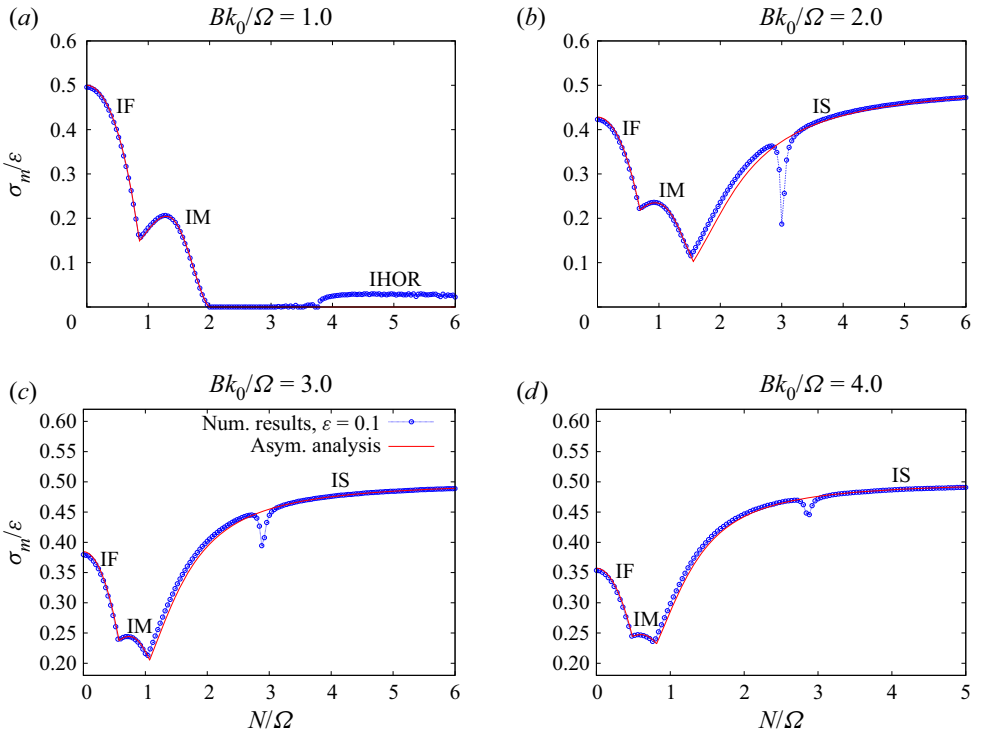

Figure 10. Magneto-gravity elliptic instabilities. Maximal growth rate of the dominant instability normalised by ε versus $\mathcal{N}$ for selected values of $\mathcal{B} = 1$ (figure 10*a*), $\mathcal{B} = 2$ (figure 10*b*), $\mathcal{B} = 3$ (figure 10*c*) and $\mathcal{B} = 4$ (figure 10*d*). The figure compares the asymptotic formulae with the numerical results at $\varepsilon = 0.1$. The subharmonic instability resulting from a resonance between two fast (respectively, slow) modes is labelled by IF (respectively, IS), whereas that resulting from a resonance between a fast and a slow mode is labelled by IM. From figure 10(*a*), we observe that an instability related to higher-order resonances (IHOR) is present for $\mathcal{N} > 3.7$.

$\mathcal{B} \gtrsim f(\mathcal{N} = 3) = 1.6035$. This can also be observed more quantitatively from figure 10 which shows σ_m/ε versus $\mathcal{N}$ for some selected values of $\mathcal{B} = 1$ (figure 10*a*), $\mathcal{B} = 2$ (figure 10*b*), $\mathcal{B} = 3$ (figure 10*c*) and $\mathcal{B} = 4$ (figure 10*d*).

A closer examination of the regions of instability in the plane $(\mu, \sigma + \varepsilon)$ for a given $(\mathcal{B}, \mathcal{N})$ belonging to the narrow band around $\mathcal{N} = 3$ reveals that beyond $\varepsilon \approx 0.1$ the subharmonic instability resulting from the resonances between two slow modes disappears and it is the instability related to resonances of order $n = 4$ between a fast mode and a slow mode which becomes dominant. This is illustrated by figure 11 which shows $\sigma + \varepsilon$ vs μ for $\mathcal{N} = 3.1$ and $\mathcal{B} = \sqrt{3}$. It can be observed that, before disappearing, the subharmonic instability coalesces with the instability related to the resonances of order $n = 6$ between two slow modes. Recall that for the identification of the different regions of instability we use (3.10) and (3.11).

Similar conclusions are drawn from the analysis of the numerical results for $0.1 < \varepsilon$ in the sense that, for $(\mathcal{B}, \mathcal{N})$ belonging to one of the domains I–VI, the dominant instability corresponds to one of the subharmonic instabilities listed in § 3. As for the agreement between the asymptotic formulae and the numerical results at $\varepsilon > 0.1$, it is not as satisfactory as in the case of weak ellipticity ($\varepsilon \lesssim 0.1$). Indeed, the difference between the numerical results and the asymptotic formulae increases as ε increases especially for

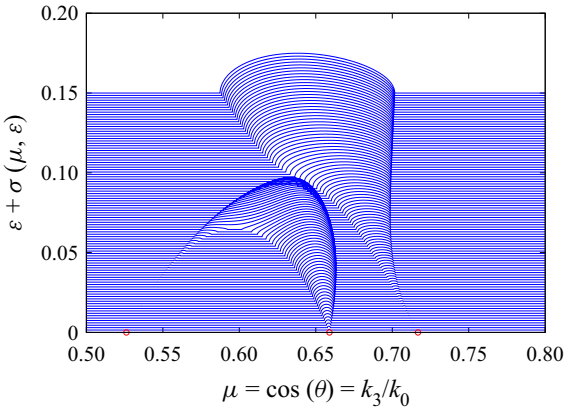

Figure 11. Magneto-gravity elliptic instabilities. The figure shows $\sigma + \varepsilon$ versus μ for $\mathcal{N} = 3.1$ and $\mathcal{B} = \sqrt{3}$, and 100 values of ε regularly distributed in the interval $0 \leq \varepsilon \leq 0.15$. The subharmonic instability IS emanates from the point $(0.6589, 0)$ and disappears beyond $\varepsilon \approx 0.1$. Before disappearing, the IS instability coalesces with the instability associated with a resonance of order $n = 6$ between two slow modes which emanates from the point $(0.5262, 0)$. The region of instability emanating from the point $(0.7168, 0)$ corresponds to the instability related to resonances of order $n = 4$ between a fast mode and a slow mode.

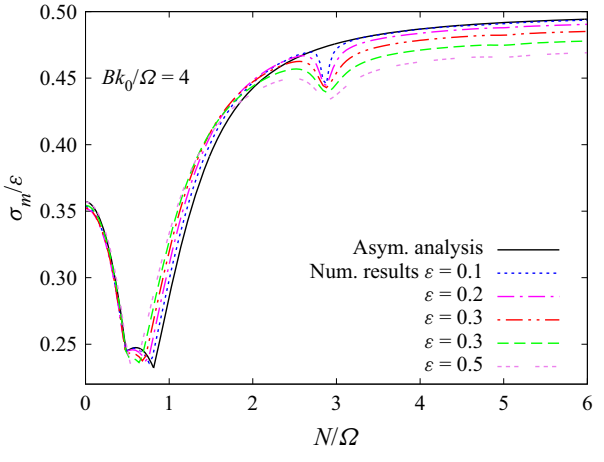

Figure 12. Magneto-gravity elliptic instabilities. Maximal growth rate of dominant instability normalised by ε versus $\mathcal{N}$ for $\varepsilon = 0.1, 0.2, 0.3, 0.4, 0.5$ and $\mathcal{B} = 4$.

$(\mathcal{B}, \mathcal{N})$ belonging to the domains V and VI. This is illustrated by figure 12 that displays σ_m/ε versus $\mathcal{N}$ for $\mathcal{B} = 4$ and five values of $\varepsilon = 0.1, 0.2, 0.3, 0.4$ and $\varepsilon = 0.5$.

We point out that the present numerical computations, as well as the asymptotic analysis, do not detect any instabilities for $2 < \mathcal{N} < 3$ and $0 \leq \mathcal{B} \leq f(\mathcal{N} = 3) = 1.6035$. As an illustration, figure 13 shows the continuous variation of the maximal growth rate σ_m of the dominant instability normalised by $\sigma_0 = 9/16$ plotted as a function of $0 \leq \mathcal{B} \leq 4$ and $0 \leq \mathcal{N} \leq 4$ for $\varepsilon = 0.5$ (figure 13*a*) and $\varepsilon = 1$ (figure 13*b*).

4.3. *Accounting for diffusivity, in the simplest case*

As indicated in the introduction, Singh & Mathur (2019) investigated the effects of differential diffusion between momentum and density ($Sc = \kappa/\nu$) in their local stability

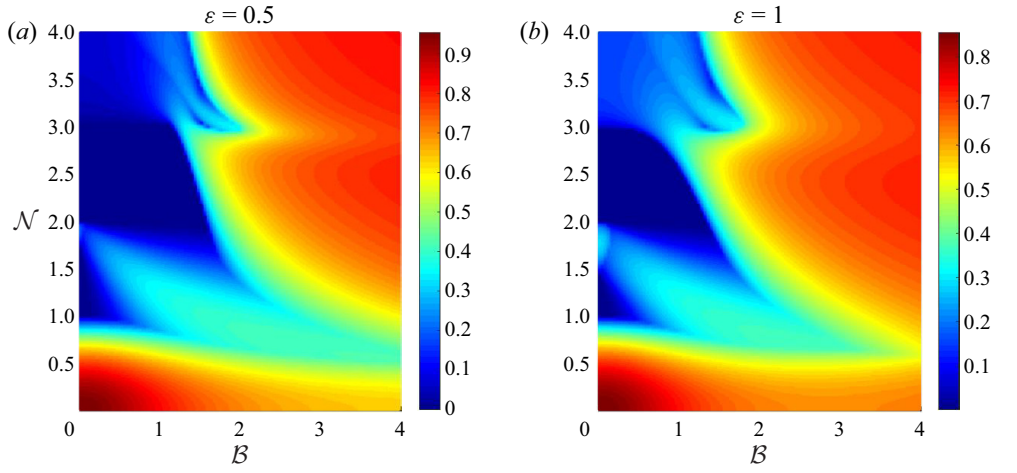

Figure 13. Magneto-gravity elliptic instabilities. Maximal growth rate of dominant instability normalised by $\sigma_0 = 9/16$ plotted as a function of $0 \leq \mathcal{B} \leq 4$ and $0 \leq \mathcal{N} \leq 4$: (*a*) $\varepsilon = 0.5$; (*b*) $\varepsilon = 1$.

analysis for an elliptical vortex with a uniform stable stratification along the vorticity axis. They showed that in the case where $Sc = \kappa/\nu = 1$ viscous effects are purely suppressive, whereas for sufficiently small $Sc < 1$, there is an oscillatory instability the signature of which is nevertheless present with zero growth rate in the inviscid limit.

The study of the effects of differential diffusion in the case of an elliptical vortex with a uniform stable stratification and a uniform magnetic field involves three dimensionless numbers, namely, the Reynolds number and the thermal and magnetic Prandtl numbers, in addition to the parameters ε, $\mathcal{B}$ and $\mathcal{N}$. This requires a detailed study and is beyond the scope of the present work. For instance, we consider the very special case where the diffusion coefficients are equal, $\nu = \kappa = \eta$.

In that case, the dispersion relation of the MIG waves is obtained by replacing ω in (3.6) by $(\omega - \nu k^2)$, and the Fourier amplitudes of the velocity, magnetic field and buoyancy scalar perturbations may be associated with those in the inviscid limit $\hat{\boldsymbol{u}}$, $\hat{\boldsymbol{b}}$ and $\hat{\vartheta}$ by the substitution (Cambon *et al.* 1985; Landman & Saffman 1987)

$$\left(\hat{\boldsymbol{u}}^{(\nu)}, \hat{\boldsymbol{b}}^{(\nu)}, \hat{\vartheta}^{(\nu)}\right) = \left(\hat{\boldsymbol{u}}, \hat{\boldsymbol{b}}, \hat{\vartheta}\right) \exp\left(-\nu \int_0^t k^2(s)\, \mathrm{d}s\right). \tag{4.3}$$

Accordingly, the maximal growth rate of the dominant instability, if attainable, is

$$\sigma_m^{(\nu)} = \sigma_m - Re^{-1} k_0^2 L_0^2 \left(1 + \frac{(E^2 - 1)(1 - \mu_m^2)}{2}\right), \tag{4.4}$$

where $Re = \Omega L_0^2/\nu$ is the Reynolds number, L_0 is a characteristic length scale and μ_m is the value of μ where σ_m occurs. At $L_0 k_0 \sim 1$, the dominant instability survives the diffusive effects if $Re > Re_c$, where

$$Re_c = \frac{2 + (E^2 - 1)(1 - \mu_m^2)}{2\sigma_m}. \tag{4.5}$$

Figure 14 shows the variation of Re_c vs $\mathcal{N}$ for $E = 1.5$ (so that $\varepsilon = 0.41667$) and $\mathcal{B} = 1, \sqrt{3}, 3$ and $\mathcal{B} = 4$. It appears that in the case where $\mathcal{B} \geq \sqrt{3}$, the dominant instability

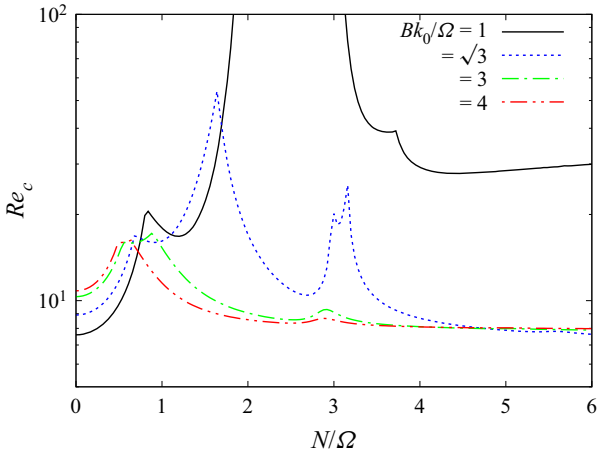

Figure 14. Case where the diffusivity coefficients (kinematic, magnetic and thermal) are equal. Variation of the critical Reynolds number Re_c versus $\mathcal{N}$ for $E = 1.5$ (therefore $\varepsilon = 0.41667$) = and $\mathcal{B} = 1$, $\sqrt{3}$, 3 and $\mathcal{B} = 4$. Dominant instability can survive the effects of diffusion, provided $Re > Re_c$.

survives the diffusion effects for $Re_c \sim 50$ and $(\mathcal{B}, \mathcal{N}) \in [\sqrt{3}, +\infty[\times [0, +\infty[$. As there are no instabilities when $2 < \mathcal{N} < 3$ and $0 < \mathcal{B} < f(\mathcal{N}) = 1.6035$, the critical Reynolds number Re_c takes large values for $\mathcal{N}$ in the left (respectively, right) neighbourhood of $\mathcal{N} = 2$ (respectively, $\mathcal{N} = 3$). This is the case for $\mathcal{B} = 1$ that we observe in figure 14.

5. Concluding remarks

We have analysed here the joint influence of a stable stratification and an external uniform magnetic field on the stability of an unbounded flow with elliptical streamlines of a perfectly conducting fluid. Both stable stratification, via the mean buoyancy gradient, and mean magnetic field are in the axial direction. Such a simple model allows us to formulate the stability problem as a system of equations for disturbances in terms of Lagrangian Fourier modes which is universal for wavelengths of the perturbation sufficiently small with respect to the scale of variation of the mean velocity gradients. Moreover, it can similarly model localised patches of elliptic streamlines which often appear in geophysical and astrophysical flows. For example, an elliptical vortex patch embedded in the accretion disc can be created by the non-uniform average angular velocity profile in the disc. Indeed, some previous studies using the zonal asymptotic method of Lifschitz & Hameiri (1991) show that these localised patches of elliptic streamlines are unstable to short-wavelength instabilities regardless of what type of flow surrounds (e.g. Lifschitz 1994; Sipp, Lauga & Jacquin 1999; Godeferd *et al.* 2001; Aravind, Dubos & Mathur 2022).

The analysis presented in the present paper extends the study by Miyazaki & Fukumoto (1992) by including the effect of the (axial) magnetic field on the gravity-elliptic instability and the study by LZ04 by including the effect of an axial stratification on the magneto-elliptic instability. The stability analysis involves a non- homogeneous Floquet system with arbitrary value of the MIPS in its right-hand side (2.25). For the purpose of the study of stability, this right-hand side ((2.25, (2.28) and (3.1)) can be set to zero without lack of generality. Of course, the resulting homogeneous Floquet system (left-hand side) already accounts for the invariance of the MIPS with parameters $(\mu, \varepsilon, k_0 B/\Omega, N/\Omega)$. This is shown by (3.6) as well.

Because most of the instabilities appearing in this elliptical flow are due to the destabilising resonances, we have analysed in detail the resonant cases of the MIG waves propagating in flows with circular streamlines ($\varepsilon = 0$). These resonant cases are of three types, the resonances between two fast modes, the resonances between a fast mode and slow mode and the resonances between two slow modes, where the last two types disappear in the absence of the unperturbed magnetic field. The asymptotic method at leading order in ε by LZ04 has been extended to determine the growth rates of the destabilising resonances of order $n = 2$ (i.e. the subharmonic instability). It results from this analysis that the subharmonic instability operates for $(k_0B/\Omega, N/\Omega)$ belonging to the domain $(]0, +\infty[\times [0, 2]) \cup ([\sqrt{3} + \infty[\times [2, +\infty[) \cup \mathcal{D}_f$ (see figure 2) where $\mathcal{D}_f$ is defined by (3.13). Moreover, the present analysis reveals that the effects of stable (axial) stratification on the magneto-elliptical instability can be analysed by distinguishing the two cases $N \leq 2\Omega$ and $N > 2\Omega$. *Case where* $0 < N \leq 2\Omega$. In that case, three subharmonic instabilities can exist: the IF (respectively, IS) instability results from resonances between two fast (slow) modes and the IM (M for mixed) instability results from resonances between a fast mode and a slow mode. For these three subharmonic instabilities, the $N \to 0$ limit is, in fact, singular (discontinuous). The IF (respectively, IM) instability is completely suppressed by stable stratification when N/Ω reaches 1 (respectively, 2), independently of the magnetic field strength. For $0 < N/\Omega < 1$ (respectively, $0 < N/\Omega < 2$) its maximal growth rate approaches zero for large k_0B, whereas in the case without stratification, it approaches $\varepsilon/4$. As for the IS instability which only occurs for $k_0B/\Omega > \sqrt{3}$, it is enhanced by the stable stratification because its maximal growth rate approaches $\varepsilon/2$ for large k_0B whereas without stratification it approaches $\varepsilon/4$. *Case where* $N/\Omega > 2$. In that case, only the subharmonic instabilities resulting from resonances between two fast modes (IF^+) or two slow modes (IS^+) can occur. The IF^+ instability can only occur for $2 < N/\Omega < +\infty$ and $1 < f(N/\Omega) \leq B/\Omega < \sqrt{3}$ (i.e. the domain $\mathcal{D}_f$). Its maximal growth rate, which approaches $\varepsilon/2$ as $k_0B/\Omega \to +\infty$, remains less than that of the IS^+ instability. On other words, for $(k_0B/\Omega, N/\Omega)$ belonging to the domain $\mathcal{D}_f$, the IS^+ instability dominates the IF^+ instability (see figure 5). The IS^+ instability is also present for $2 < N/\Omega < +\infty$ and $\sqrt{3} < k_0B/\Omega < +\infty$ with a maximal growth rate approaching $\varepsilon/2$ for large k_0B. Note that the enhancement of the IS instability when the two backgrounds are simultaneously present is connected with a large exchange of energy between the kinetic and magnetic energies and between the kinetic and potential energies.

The analytical results were compared with numerical results for several values of $0 \leq \varepsilon \leq 1$, $0 \leq \mathcal{B} \leq 4$ and $0 \leq \mathcal{N} \leq 4$. The comparison reveals that the subharmonic instability, if it exists, dominates the instabilities related to higher-order resonances ($n = 4, 6, 8, \ldots$). The agreement between the asymptotic formulae and the numerical results is quite good for small ellipticities ($\varepsilon \lesssim 0.1$) (see figure 12). The numerical results also reveal that for a narrow band around $\mathcal{N} = 3$, the dominant instability is rather that related to resonances of order $n = 4$ between a fast mode and a slow mode (see figure 11). Instabilities related to higher-order resonances can occur for $(\mathcal{B}, \mathcal{N}) \in [0, \sqrt{3}[\times]2, \infty[\backslash \mathcal{D}_f$ (see, e.g., figure 8).

The whole analysis developed in this study is essentially linear, and linearisation deserves some discussion. On the one hand, it was clarified that a two-mode analysis is needed for the destabilising resonances, in contrast with a single-mode analysis where the nonlinearity is identically zero (Craik & Criminale 1986; Moffatt 2010). Other cases where the nonlinearity is not explicit, but implicitly present, exist in the literature, especially in astrophysics, with the regeneration of modes for bypass transition in accretion discs (e.g.

Chagelishvili *et al.* 2003). Looking at the velocity field, linearisation cannot be justified by a small value of the perturbed velocity field with respect to the base (mean) velocity field, which is extensional: a ratio of time scale is used instead in the so-called RDT as the linear 'rapid' limit; a typical time-scale of the 'turbulent' velocity field is assumed to be large with respect to the time scale given by the (inverse of the magnitude of) the mean velocity gradients (e.g. $\boldsymbol{A}$ in (2.6*a*)). As suggested by an anonymous referee, some robustness of the linear solution results from the particular mean flow configuration, where the periods of a fluid element moving along different streamlines are the same. Accordingly, there is no growth of gradient, as a source of nonlinearity, and thereby of wavenumber, across the streamlines direction.

The present analysis, which allowed us to map the domains of the $(\mathcal{B}, \mathcal{N})$ space for which the magneto-gravity-elliptic instability can operate, would serve to guide future DNS for the study of the effects of nonlinearity on this instability. Note that, in the case of the magneto-precessional instability, the regime of the saturation of this instability by nonlinear interactions was identified. It corresponds to a saturation stage during which the total turbulent energy (kinetic + magnetic), the production rate due to the base flow and the total dissipation rate remain almost independent of time where the dissipation rate balances the production rate (Salhi, Khlifi & Cambon 2020).

The question that can arise concerns the joint influence of Lorentz, Coriolis and buoyancy forces on the elliptical instability. With the inclusion of the Coriolis force, in addition to the Lorentz and buoyancy forces, the problem turns out to be more complex because the resulting fourth four-component linear Floquet system becomes one with five parameters, namely $(\mu, \varepsilon, \mathcal{B}, \mathcal{N}, \Omega_c/\Omega)$, ($\Omega_c$ being the angular velocity of system rotation). For that we preferred not to include, in this analysis, the effect of the Coriolis force.

As a useful extension of our present study, more complex but with a similar analysis, an additional Coriolis force can be introduced. Keeping the same effects of stratified MHD, the problem will include the angular velocity Ω_c of the system rotation in addition to the basic angular velocity Ω. Moreover, for anticyclonic rotation (i.e.$\Omega_c \leq -\Gamma/2 = -\Omega(E + E^{-1})/4$), the horizontal instability is dominant Bajer & Mizerski 2013). Indeed, when the wave vector is axial (here, the vectors $\boldsymbol{\Omega}_c$, $\boldsymbol{B}$ and $\boldsymbol{\nabla}\varrho$ are also axial) there is no effect of the buoyancy force (in the linear regime) since the frequency of gravity waves is zero ($\omega_g = 0$). In that case, the maximal growth rate of the horizontal instability, which is not of resonant nature, is about $\sigma_m/\varepsilon = 1$ for $(k_3 B)^2 = -\Omega^2(1 + 2\Omega_c/\Omega)$ in the limit of small ε (so that, $\Gamma = \Omega(1 + O(\varepsilon^2))$. The study of the effect of cyclonic rotation on the magneto-gravity-elliptic instability, as well as the study of the joint influence of a stable stratification and unperturbed magnetic field on the precessional instability, are the subject of future studies.

Declaration of interests. The authors report no conflict of interest.

Author ORCIDs.
Abdelaziz Salhi https://orcid.org/0000-0002-3154-345X;
Claude Cambon https://orcid.org/0000-0002-6825-5195.

Appendix A. Asymptotic analysis at leading order in ε of the Floquet system (2.28)

In this appendix, we extend the asymptotic method of LZ04 to determine, at leading order in ε, the maximal growth rate of the solution of the four-component Floquet system (2.28),

$d_\tau \hat{\boldsymbol{c}} = \boldsymbol{D} \cdot \hat{\boldsymbol{c}}$. Recall that $\boldsymbol{\Phi}(\tau, \varepsilon, \mu, \mathcal{B}, \mathcal{N})$ denotes the fundamental matrix solution,

$$d_\tau \boldsymbol{\Phi} = \boldsymbol{D} \cdot \boldsymbol{\Phi}, \quad \boldsymbol{\Phi}(\tau = 0) = \boldsymbol{I}_4 \tag{A1a,b}$$

and $\boldsymbol{M} = \boldsymbol{\Phi}(2\pi, \varepsilon, \mu, \mathcal{B}, \mathcal{N})$ denotes the Floquet multiplier matrix where its determinant is unity (see the end of § 2.3). It follows that whenever λ is an eigenvalue of $\boldsymbol{M}$, so also are its inverse λ^{-1} and its complex conjugate λ^*. We denote by

$$p(\lambda, \varepsilon) = |\boldsymbol{M} - \lambda \boldsymbol{I}_4| \tag{A2}$$

the characteristic polynomial of the characteristic polynomial of the Floquet multiplier matrix $\boldsymbol{M}$ and by Λ_1, Λ_2, Λ_3 and Λ_4 its roots. A necessary condition for stability is that each root lie on the unit circle (see LZ04).

A.1. *Expansion in Taylor series of the Floquet multiplier matrix*

We expand the Floquet multiplier matrix $\boldsymbol{M}(\varepsilon, \mu, \mathcal{B}, \mathcal{N})$ in Taylor series in the neighbourhood of $(\varepsilon, \mu) = (0, \mu_0)$, holding $(\mathcal{B}, \mathcal{N})$ constant,

$$\boldsymbol{M} = \boldsymbol{M}_0(\mu_0, 0) + \varepsilon \boldsymbol{M}_\varepsilon(\mu_0, 0) + (\mu - \mu_0)\boldsymbol{M}_\mu(\mu_0, 0) + \cdots, \tag{A3}$$

where $\boldsymbol{M}_\varepsilon = (\partial \boldsymbol{M}/\partial \varepsilon)$, $\boldsymbol{M}_\mu = (\partial \boldsymbol{M}/\partial \mu)$ and the dots indicate higher-order terms in ε and $\mu - \mu_0$. In general, at sufficiently small ε, the region in the (ε, μ) plane where instability occurs is typically a wedge with apex at a point $(\varepsilon, \mu) = (0, \mu_0)$ and boundaries

$$\mu = \mu_0 + \gamma_\pm \varepsilon, \tag{A4}$$

where the slopes γ_+ and γ_- are to be found. The instability (if it exists) has a bandwidth $(\gamma_+ - \gamma_-)\varepsilon$; that is, for given ε, $\mathcal{B}$ and $\mathcal{N}$, the length of the $\mu-$interval for which the wavenumbers are unstable. Therefore, (A3) can be rewritten as

$$\boldsymbol{M} = \boldsymbol{M}_0 + \varepsilon \boldsymbol{M}_1 + O(\varepsilon^2), \tag{A5a}$$

$$\boldsymbol{M}_1 = \boldsymbol{M}_\varepsilon + \gamma \boldsymbol{M} \mu. \tag{A5b}$$

Accordingly, we no longer need the designation μ_0 and, hereinafter, use the symbol μ in its place.

To determine matrices $\boldsymbol{M}_0$, $\boldsymbol{M}_\varepsilon$ and $\boldsymbol{M}_\mu$, we expand, for a given $\tau \in [0, 2\pi]$, $\boldsymbol{\Phi}$ and $\boldsymbol{D}$,

$$\boldsymbol{\Phi}(\tau, \varepsilon) = \boldsymbol{\Phi}_0(\tau, \mu, 0) + \varepsilon \boldsymbol{\Phi}_1(\tau, \mu, 0) + O(\varepsilon^2), \tag{A6a}$$

$$\boldsymbol{D}(\tau, \varepsilon) = \boldsymbol{D}_0 + \varepsilon \boldsymbol{D}_\varepsilon(\tau, 0) + O(\varepsilon^2), \tag{A6b}$$

where $\boldsymbol{\Phi}_0(\tau = 0) = \boldsymbol{I}_4$ and $\boldsymbol{\Phi}_1(\tau = 0) = \boldsymbol{0}$. Substituting (A6) into (A1a,b), we obtain

$$d_\tau \boldsymbol{\Phi}_0 = \boldsymbol{D}_0 \cdot \boldsymbol{\Phi}_0, \quad d_\tau \boldsymbol{\Phi}_1 = \boldsymbol{D}_0 \cdot \boldsymbol{\Phi}_1 + \boldsymbol{D}_\varepsilon \cdot \boldsymbol{\Phi}_0, \tag{A7a,b}$$

with solution $\boldsymbol{\Phi}_0(\tau) = \mathrm{e}^{\tau \boldsymbol{D}_0}$ and

$$\boldsymbol{\Phi}_1(\tau) = \boldsymbol{\Phi}_0(\tau) \cdot \left(\int_0^\tau \boldsymbol{\Phi}_0^{-1}(s) \cdot \boldsymbol{D}_\varepsilon(s) \cdot \boldsymbol{\Phi}_0(s) \, \mathrm{d}s \right). \tag{A8}$$

Because the characteristic polynomial $p(\lambda, \varepsilon)$ is the same in any coordinate system and the four eigenvalues of the matrix $\boldsymbol{D}_0$, given by (3.6) (repeated here for the sake of clarity)

are distinct

$$\sigma_1 = -\sigma_2 = -\frac{\mathrm{i}}{\sqrt{2}}\sqrt{\left(4+2\mathcal{B}^2-\mathcal{N}^2\right)\mu^2+\mathcal{N}^2+\sqrt{\left[\left(4-\mathcal{N}^2\right)\mu^2+\mathcal{N}^2\right]^2+16\mathcal{B}^2\mu^4}} \tag{A9a}$$

$$\sigma_3 = -\sigma_4 = -\frac{\mathrm{i}}{\sqrt{2}}\sqrt{\left(4+2\mathcal{B}^2-\mathcal{N}^2\right)\mu^2+\mathcal{N}^2-\sqrt{\left[\left(4-\mathcal{N}^2\right)\mu^2+\mathcal{N}^2\right]^2+16\mathcal{B}^2\mu^4}} \tag{A9b}$$

as long as $\mathcal{B}\neq 0$ and $0<\mu^2<1$, we transform the solution in the base diagonalising $\boldsymbol{D}_0$,

$$\tilde{\boldsymbol{D}}_0 = \boldsymbol{T}^{-1}\cdot\boldsymbol{D}_0\cdot\boldsymbol{T} = \mathrm{diag}\left(\sigma_1,-\sigma_1,\sigma_3,-\sigma_3\right). \tag{A10}$$

Here, the columns of $\boldsymbol{T}$ are the eigenvectors of $\boldsymbol{D}_0$,

$$\boldsymbol{T} = \begin{pmatrix} \sigma_1 & -\sigma_1 & \sigma_3 & -\sigma_3 \\ -\frac{1}{2}\left(\sigma_1^2+m^2\right) & -\frac{1}{2}\left(\sigma_1^2+m^2\right) & -\frac{1}{2}\left(\sigma_3^2+m^2\right) & -\frac{1}{2}\left(\sigma_3^2+m^2\right) \\ \mathrm{i}m & \mathrm{i}m & \mathrm{i}m & \mathrm{i}m \\ -\frac{\mathrm{i}}{2}\frac{m}{\sigma_1}\left(\sigma_1^2+m^2\right) & \frac{\mathrm{i}}{2}\frac{m}{\sigma_1}\left(\sigma_1^2+m^2\right) & -\frac{\mathrm{i}}{2}\frac{m}{\sigma_3}\left(\sigma_3^2+m^2\right) & \frac{\mathrm{i}}{2}\frac{m}{\sigma_3}\left(\sigma_3^2+m^2\right) \end{pmatrix} \tag{A11}$$

$$\boldsymbol{T}^{-1} = \frac{1}{\left(\sigma_1^2-\sigma_3^2\right)}\begin{pmatrix} \frac{1}{2}\frac{\sigma_1}{m^2}\left(\sigma_3^2+m^2\right) & -1 & \frac{\mathrm{i}}{2m}\left(\sigma_3^2+m^2\right) & -\frac{\mathrm{i}\sigma_1\sigma_3^2}{m^3} \\ -\frac{1}{2}\frac{\sigma_1}{m^2}\left(\sigma_3^2+m^2\right) & -1 & \frac{\mathrm{i}}{2m}\left(\sigma_3^2+m^2\right) & \frac{\mathrm{i}\sigma_1\sigma_3^2}{m^3} \\ -\frac{1}{2}\frac{\sigma_3}{m^2}\left(\sigma_1^2+m^2\right) & 1 & -\frac{\mathrm{i}}{2m}\left(\sigma_1^2+m^2\right) & \frac{\mathrm{i}\sigma_3\sigma_1^2}{m^3} \\ \frac{1}{2}\frac{\sigma_3}{m^2}\left(\sigma_1^2+m^2\right) & 1 & -\frac{\mathrm{i}}{2m}\left(\sigma_1^2+m^2\right) & -\frac{\mathrm{i}\sigma_3\sigma_1^2}{m^3} \end{pmatrix}, \tag{A12}$$

where $m=\mathcal{B}\mu$. Therefore, in the base diagonalising $\boldsymbol{D}_0$, $\tilde{\boldsymbol{M}}_0$ and $\tilde{\boldsymbol{M}}_\varepsilon$ take the form

$$\tilde{\boldsymbol{M}}_0 = \boldsymbol{T}^{-1}\cdot\boldsymbol{M}_0\cdot\boldsymbol{T} = \mathrm{diag}\left(\mathrm{e}^{2\pi\sigma_1},\mathrm{e}^{-2\pi\sigma_1},\mathrm{e}^{2\pi\sigma_3},\mathrm{e}^{-2\pi\sigma_3}\right) = \mathrm{diag}\left(\lambda_1,\lambda_2,\lambda_3,\lambda_4\right), \tag{A13a}$$

$$\tilde{\boldsymbol{M}}_\varepsilon = \boldsymbol{T}^{-1}\cdot\boldsymbol{M}_\varepsilon\cdot\boldsymbol{T} = \tilde{\boldsymbol{M}}_0\cdot\tilde{\boldsymbol{J}}, \tag{A13b}$$

$$\tilde{J}_{ij} = \left(\boldsymbol{T}^{-1}\right)_{im} T_{lj}\int_0^{2\pi}\mathrm{e}^{(\sigma_j-\sigma_i)\tau}\left(\boldsymbol{D}_\varepsilon\right)_{ml}(\tau)\,\mathrm{d}\tau. \tag{A13c}$$

To complete the construction of the matrix $\tilde{\boldsymbol{M}}_1$, which appears in (A5), we need the derivative of $\tilde{\boldsymbol{M}}_0(\mu)=\tilde{\boldsymbol{M}}(\mu,0)$ with respect to μ,

$$\gamma\tilde{\boldsymbol{M}}_\mu = \gamma\frac{\partial\tilde{\boldsymbol{M}}_0}{\partial\mu} = \frac{2\mathrm{i}\pi\gamma}{\Omega}\,\mathrm{diag}\left(\frac{\partial\omega_1}{\partial\mu}\lambda_1,\frac{\partial\omega_2}{\partial\mu}\lambda_2,\frac{\partial\omega_3}{\partial\mu}\lambda_3,\frac{\partial\omega_4}{\partial\mu}\lambda_4\right). \tag{A14}$$

A.2. *Expansion of the characteristic polynomial*

We expand the characteristic polynomial in Taylor series around $\varepsilon = 0$ to second order in ε,

$$p(\lambda, \varepsilon) = p_0(\lambda) + p_1(\lambda)\varepsilon + p_2(\lambda)\varepsilon^2 + O\left(\varepsilon^3\right), \tag{A15}$$

where $p_0(\lambda)$ is the characteristic polynomial of $\boldsymbol{M}_0$ with roots $\lambda_1 = \mathrm{e}^{2\pi\sigma_1}$, $\lambda_2 = \mathrm{e}^{-2\pi\sigma_1}$, $\lambda_3 = \mathrm{e}^{2\pi\sigma_3}$ and $\lambda_4 = \mathrm{e}^{-2\pi\sigma_3}$. Although $\sigma_1, \sigma_2, \sigma_3$ and σ_4 are distinct, it is possible for the multipliers λ_j ($j = 1, 2, 3, 4$) to be repeated: if $\sigma_j - \sigma_m = \mathrm{i}\ell$ for an integer $\ell \neq 0$, then $\lambda_j = \lambda_m$. As shown by LZ04, a necessary condition for the onset of instability is that there be a double (or higher) root of the characteristic equation. As we only consider the case in which the eigenvalues are multiplicity 2, the Puiseux expansion takes the form

$$\Lambda_1 = \lambda_1 + \varepsilon^{1/2}\beta_{\frac{1}{2}} + \varepsilon\beta_1 + O\left(\varepsilon^{3/2}\right), \tag{A16}$$

where, for definiteness, we have assumed that $\lambda_1 = \lambda_2$. It can be shown, however, that $\beta_{1/2} = 0$, in this case, and then the leading-order correction to the eigenvalue, $\beta_1 \neq 0$, can be established from a quadratic equation

$$\frac{1}{2}\left[\frac{\mathrm{d}^2 p_0}{\mathrm{d}\lambda^2}(\lambda_1)\right]\beta_1^2 + \left[\frac{\mathrm{d}p_1}{\mathrm{d}\lambda}(\lambda_1)\right]\beta_1 + p_2(\lambda_1) = 0. \tag{A17}$$

By the use of the formulae for the derivatives of the characteristic polynomial with respect to parameter ε, derived by LZ04 (see their appendix B), we obtain

$$\frac{\mathrm{d}^2 p_0}{\mathrm{d}\lambda^2}(\lambda_1) = 2\left(\lambda_3 - \lambda_1\right)\left(\lambda_4 - \lambda_1\right), \tag{A18a}$$

$$p_1(\lambda_1) = \sum_{j=1}^{4}\left(\tilde{\boldsymbol{M}}_1\right)_{jj}\prod_{\ell \neq j}\left(\lambda_\ell - \lambda\right), \tag{A18b}$$

$$\frac{\mathrm{d}p_1}{\mathrm{d}\lambda}(\lambda_1) = \left[\left(\tilde{\boldsymbol{M}}_1\right)_{11} + \left(\tilde{\boldsymbol{M}}_1\right)_{22}\right]\left(\lambda_3 - \lambda_1\right)\left(\lambda_4 - \lambda_1\right), \tag{A18c}$$

$$p_2(\lambda_1) = \begin{vmatrix} \left(\tilde{\boldsymbol{M}}_1\right)_{11} & \left(\tilde{\boldsymbol{M}}_1\right)_{12} \\ \left(\tilde{\boldsymbol{M}}_1\right)_{21} & \left(\tilde{\boldsymbol{M}}_1\right)_{22} \end{vmatrix}\left(\lambda_3 - \lambda_1\right)\left(\lambda_4 - \lambda_1\right). \tag{A18d}$$

Going back to the general case of $\lambda_j = \lambda_m$, the quadratic equation (A17), with the aid of (A5*b*), (A13) and (A18) can easily be transformed to an equation for the coefficient $\alpha = \beta/\lambda_j$,

$$\alpha^2 - \left(\tilde{J}_{jj} + \tilde{J}_{mm} + \frac{2\mathrm{i}\pi\gamma}{\Omega}\left(\frac{\partial\omega_j}{\partial\mu} + \frac{\partial\omega_m}{\partial\mu}\right)\right)\alpha + \begin{vmatrix} \tilde{J}_{jj} + \dfrac{2\mathrm{i}\pi\gamma}{\Omega}\dfrac{\partial\omega_j}{\partial\mu} & \tilde{J}_{jm} \\ \tilde{J}_{mj} & \tilde{J}_{mm} + \dfrac{2\mathrm{i}\pi\gamma}{\Omega}\dfrac{\partial\omega_m}{\partial\mu} \end{vmatrix} = 0. \tag{A19}$$

Therefore, either α is pure imaginary and we infer stability (to leading order in ε), or $\mathrm{Re}\,\alpha \neq 0$ and we infer instability (see Proposition 2 in LZ04).

A.3. *Maximal growth rates of subharmonic instabilities*

The solutions of the quadratic equation (A19) take the form,

$$\alpha = \frac{1}{2}\left[\tilde{J}_{jj} + \tilde{J}_{mm} + \frac{2\mathrm{i}\pi\gamma}{\Omega}\left(\frac{\partial\omega_j}{\partial\mu} + \frac{\partial\omega_m}{\partial\mu}\right)\right] \pm \frac{1}{2}\sqrt{D}, \tag{A20}$$

where the expression for D can be put in the form

$$D = -\left|\tilde{J}_{jj} - \tilde{J}_{mm} + \frac{2\mathrm{i}\pi\gamma}{\Omega}\left(\frac{\partial\omega_j}{\partial\mu} - \frac{\partial\omega_m}{\partial\mu}\right)\right|^2 + 4\tilde{J}_{jm}\tilde{J}_{mj}, \tag{A21}$$

because all the diagonal elements of the matrix $\tilde{\boldsymbol{J}}$ are pure-imaginary numbers. The discriminant D must be greater than zero in order to have instability, so that

$$4\tilde{J}_{jm}\tilde{J}_{mj} > \left|\tilde{J}_{jj} - \tilde{J}_{mm} + \frac{2\mathrm{i}\pi\gamma}{\Omega}\left(\frac{\partial\omega_j}{\partial\mu} - \frac{\partial\omega_m}{\partial\mu}\right)\right|^2 > 0. \tag{A22}$$

Now the maximal growth rate, which in this case is achieved for

$$\gamma = \frac{\mathrm{i}\Omega\left(\tilde{J}_{jj} - \tilde{J}_{mm}\right)}{2\pi\left(\dfrac{\partial\omega_j}{\partial\mu} - \dfrac{\partial\omega_m}{\partial\mu}\right)} \in \mathbb{R} \tag{A23}$$

is

$$\sigma_{max} = \frac{\varepsilon}{2\pi}\left(\mathrm{Re}\,\alpha\right)_{max} = \frac{\varepsilon}{2\pi}\sqrt{\tilde{J}_{jm}\tilde{J}_{mj}} \quad (\text{with } j \neq m). \tag{A24}$$

We now show that the diagonal elements of the matrix $\tilde{\boldsymbol{J}}$ are pure-imaginary numbers.

From (2.26) giving the matrix $\boldsymbol{D}$, we deduce $\boldsymbol{D}_\varepsilon$, where its non-zero elements are

$$(\boldsymbol{D}_\varepsilon)_{11} = \mathrm{i}\left(1-\mu^2\right)\left(\mathrm{e}^{2\mathrm{i}\tau} - \mathrm{e}^{-2\mathrm{i}\tau}\right), \tag{A25a}$$

$$(\boldsymbol{D}_\varepsilon)_{14} = \frac{\mathcal{N}^2}{2\mathcal{B}}\frac{\left(1-\mu^2\right)}{\mu}\left(\mathrm{e}^{2\mathrm{i}\tau} - \mathrm{e}^{-2\mathrm{i}\tau}\right), \tag{A25b}$$

$$(\boldsymbol{D}_\varepsilon)_{21} = \mu^2\left(1-\mu^2\right)\left(\mathrm{e}^{2\mathrm{i}\tau} + \mathrm{e}^{-2\mathrm{i}\tau} - 2\right), \tag{A25c}$$

$$(\boldsymbol{D}_\varepsilon)_{24} = -\mathrm{i}\frac{\mathcal{N}^2}{2\mathcal{B}}\mu\left(1-\mu^2\right)\left(\mathrm{e}^{2\mathrm{i}\tau} + \mathrm{e}^{-2\mathrm{i}\tau} - 2\right). \tag{A25d}$$

Substituting the above expressions into (A13c) and using (A11) and (A12) we obtain

$$\tilde{J}_{jj} = \left(\mathbf{T}^{-1}\right)_{j2}\left(T_{1j}\int_0^{2\pi}(\mathbf{D}_\varepsilon)_{21}\,\mathrm{d}\tau + T_{4j}\int_0^{2\pi}(\mathbf{D}_\varepsilon)_{24}\,\mathrm{d}\tau\right), \tag{A26a}$$

$$\tilde{J}_{11} = -\tilde{J}_{22} = \mathrm{i}\pi\mu^2\left(1-\mu^2\right)\frac{\left(4-\mathcal{N}^2\right)\omega_1^2 + \mathcal{N}^2\mathcal{B}^2\mu^2}{\omega_1\left(\omega_3^2 - \omega_1^2\right)}, \tag{A26b}$$

$$\tilde{J}_{33} = -\tilde{J}_{44} = -\mathrm{i}\pi\mu^2\left(1-\mu^2\right)\frac{\left(4-\mathcal{N}^2\right)\omega_3^2 + \mathcal{N}^2\mathcal{B}^2\mu^2}{\omega_3\left(\omega_3^2 - \omega_1^2\right)}, \tag{A26c}$$

in which, as well as throughout the remainder of this appendix, the frequencies ω_1 and ω_3 are normalised by Ω. Equation (A26) proves that the diagonal elements of the matrix

$\tilde{\boldsymbol{J}}$ are pure-imaginary numbers. This implies that the slopes $\gamma_{\pm}$, which are solutions of the equation $\mathrm{Re}(\alpha) = 0$, are also solutions of the equation $\mathrm{Re}(\sqrt{D}) = 0$. The expression of D given by (A21) involves the term $(\partial_\mu \omega_j - \partial_\mu \omega_m)$. However, the dependence of the frequencies ω_j and ω_m on the variable μ is not linear which increases the complexity of an analytical development in the resolution of $\mathrm{Re}(\sqrt{D}) = 0$. It appears more convenient to perform analytically the derivatives $\partial_\mu \omega_j$ and $\partial_\mu \omega_m$, and to resolve numerically the equation $\mathrm{Re}(\sqrt{D}) = 0$.

We now calculate the maximal growth rates associated with the three unstable cases, namely the fast–fast (case 1), slow–slow (case 2) and fast–slow (case 3) destabilising resonances.

A.3.1. *Case 1*

The frequencies ω_1 and $\omega_2 = -\omega_1$ given by (3.4*a*) correspond to fast modes and a resonance (or order $n = 2$) between them is characterised by $\omega_1 - \omega_2 = 2$, so

$$\omega_1 = -\omega_2 = 1 \quad \text{or} \quad \sigma_1 = -\sigma_2 = \mathrm{i}. \tag{A27}$$

The maximal growth rate of the subharmonic instability IF, denoted by σ_{mf}, is described by (A24) which, in this case, reduces to

$$\sigma_{mf} = \frac{\varepsilon}{2\pi} (\mathrm{Re}\,\alpha)_{max} = \frac{\varepsilon}{2\pi} \sqrt{\tilde{J}_{12}\tilde{J}_{21}} \tag{A28}$$

with

$$\tilde{J}_{12} = \left(\boldsymbol{T}^{-1}\right)_{1m} T_{n2} \int_0^{2\pi} \mathrm{e}^{-2\mathrm{i}\tau} \, (\boldsymbol{D}_\varepsilon)_{mn} \, \mathrm{d}\tau = \left(\boldsymbol{T}^{-1}\right)_{1m} T_{n2} H^{+}_{mn} \tag{A29}$$

$$\tilde{J}_{21} = \left(\boldsymbol{T}^{-1}\right)_{2m} T_{n1} \int_0^{2\pi} \mathrm{e}^{+2\mathrm{i}\tau} \, (\boldsymbol{D}_\varepsilon)_{mn} \, \mathrm{d}\tau = \left(\boldsymbol{T}^{-1}\right)_{2m} T_{n1} H^{-}_{mn}, \tag{A30}$$

where, given (A25), the non-zero elements H^{+}_{mn} and H^{-}_{mn} take the form

$$H^{+}_{11} = -H^{-}_{11} = 2\mathrm{i}\pi(1-\mu^2), \tag{A31a}$$

$$H^{+}_{14} = -H^{-}_{14} = \pi \frac{\mathcal{N}^2}{\mathcal{B}} \frac{(1-\mu^2)}{\mu}, \tag{A31b}$$

$$H^{+}_{21} = H^{-}_{21} = 2\pi\mu^2(1-\mu^2), \tag{A31c}$$

$$H^{+}_{24} = H^{-}_{24} = -\mathrm{i}\pi \frac{\mathcal{N}^2}{\mathcal{B}} \mu(1-\mu^2). \tag{A31d}$$

With the aid of (A11) and (A12) one easily shows that $\tilde{J}_{21} = -\tilde{J}_{12}$. Now back to determining the element $\tilde{J}_{12}$

$$\tilde{J}_{12} = \left(\boldsymbol{T}^{-1}\right)_{11} \left(H^{+}_{11} T_{12} + H^{+}_{14} T_{42}\right) + \left(\boldsymbol{T}^{-1}\right)_{12} \left(H^{+}_{21} T_{12} + H^{+}_{24} T_{42}\right). \tag{A32}$$

The substitution of $\boldsymbol{T}^{-1}_{ij}$, H^{+}_{ij} and T_{ij} by their expressions respectively given by (A12), (A31) and (A11) into (A32) leads to

$$\tilde{J}_{12} = -\tilde{J}_{21} = -\frac{\mathrm{i}\pi}{4} \frac{(1-\mu^2)}{(1-\omega_3^2)} \left(4 - \mathcal{N}^2 + \mathcal{B}^2\mathcal{N}^2\mu^2\right) \left(1 + 2\mu^2 - \frac{\omega_3^2}{\mathcal{B}^2\mu^2}\right). \tag{A33}$$

From (3.4*a*) and (3.4*b*) giving the expression of the frequencies ω_1 and ω_3, we deduce that

$$\omega_1^2+\omega_3^2=1+\omega_3^2=\left(4+2\mathcal{B}^2-\mathcal{N}^2\right)\mu^2+\mathcal{N}^2 \tag{A34}$$

because $\omega_1=1$ in case 1. Moreover, with the aid of the resonance condition (3.10), we deduce the equality

$$\omega_3^2=\left(4+2\mathcal{B}^2-\mathcal{N}^2\right)\mu^2+\mathcal{N}^2-1=\mathcal{B}^2\mu^2\left[\left(\mathcal{B}^2-\mathcal{N}^2\right)\mu^2+1\right]. \tag{A35}$$

Accordingly, the substitution of (A35) into (A33) leads to

$$\tilde{J}_{12}=-\tilde{J}_{21}=-\frac{\mathrm{i}\pi}{4}\left(3-\mathcal{B}^2\mu^2\right)\left(1+\mathcal{B}^2\mu^2\right)\frac{\left[\left(\mathcal{N}^2-\mathcal{B}^2+2\right)\mu^2+\left(1-\mathcal{N}^2\right)\right]}{\left[\left(\mathcal{N}^2-2\mathcal{B}^2-4\right)\mu^2+\left(2-\mathcal{N}^2\right)\right]}. \tag{A36}$$

Hence, we obtain the expression of

$$\frac{\sigma_{mf}}{\varepsilon}=\frac{1}{2\pi}\left(\mathrm{Re}\,\alpha\right)_{max}=\frac{1}{2\pi}\sqrt{\tilde{J}_{12}\tilde{J}_{21}}=\sqrt{-\left(\tilde{J}_{12}\right)^2}\geq 0 \tag{A37}$$

given by (3.18) in which the parameter μ is given by (3.15).

A.3.2. *Case 2*

The frequencies ω_3 and $\omega_4=-\omega_3$ given by (3.4*b*) correspond to slow modes and a resonance (or order $n=2$) between them is characterised by $\omega_3-\omega_4=2$, so

$$\omega_3=-\omega_4=1 \quad \text{or} \quad \sigma_3=-\sigma_4=\mathrm{i}. \tag{A38}$$

The maximal growth rate of the subharmonic instability IS, denoted by σ_{ms}, is then described by (A24) which, in this case, reduces to

$$\sigma_{ms}=\frac{\varepsilon}{2\pi}\left(\mathrm{Re}\,\alpha\right)_{max}=\frac{\varepsilon}{2\pi}\sqrt{\tilde{J}_{34}\tilde{J}_{43}}. \tag{A39}$$

With the aid of (A11) and (A12) we show that $\tilde{J}_{43}=-\tilde{J}_{34}$. The determination of the element

$$\tilde{J}_{34}=\left(\boldsymbol{T}^{-1}\right)_{31}\left(H_{11}^{+}T_{12}+H_{14}^{+}T_{44}\right)+\left(\boldsymbol{T}^{-1}\right)_{32}\left(H_{21}^{+}T_{14}+H_{24}^{+}T_{44}\right) \tag{A40}$$

is similar to that of $\tilde{J}_{12}$ since if we perform the permutation $\sigma_1\leftrightarrow\sigma_3$ in the expression of $\left(\boldsymbol{T}^{-1}\right)_{11}$, $\left(\boldsymbol{T}^{-1}\right)_{12}$, T_{12} and T_{42} in (A11) and (A12) we obtain the expression of $\left(\boldsymbol{T}^{-1}\right)_{31}$, $\left(\boldsymbol{T}^{-1}\right)_{32}$, T_{14} and T_{44} and, hence,

$$\tilde{J}_{34}=-\tilde{J}_{43}=-\frac{\mathrm{i}\pi}{4}\frac{\left(1-\mu^2\right)}{\left(1-\omega_1^2\right)}\left(4-\mathcal{N}^2+\mathcal{B}^2\mathcal{N}^2\mu^2\right)\left(1+2\mu^2-\frac{\omega_1^2}{\mathcal{B}^2\mu^2}\right), \tag{A41}$$

where

$$\omega_1^2=\left(4+2\mathcal{B}^2-\mathcal{N}^2\right)\mu^2+\mathcal{N}^2-1=\mathcal{B}^2\mu^2\left[\left(\mathcal{B}^2-\mathcal{N}^2\right)\mu^2+1\right]. \tag{A42}$$

Thus, the substitution of (A42) into (A43) gives rise to

$$\tilde{J}_{34}=-\tilde{J}_{43}=-\frac{\mathrm{i}\pi}{4}\left(3-\mathcal{B}^2\mu^2\right)\left(1+\mathcal{B}^2\mu^2\right)\frac{\left[\left(\mathcal{N}^2-\mathcal{B}^2+2\right)\mu^2+\left(1-\mathcal{N}^2\right)\right]}{\left[\left(\mathcal{N}^2-2\mathcal{B}^2-4\right)\mu^2+\left(2-\mathcal{N}^2\right)\right]}, \tag{A43}$$

which is identical to (A36). The difference is due to the fact that, in (A36), the parameter μ is described by (3.15), whereas in (A43) it is given by (3.25). It then results in

the expression

$$\frac{\sigma_{ms}}{\varepsilon} = \frac{1}{2\pi}\left(\mathrm{Re}\,\alpha\right)_{max} = \frac{1}{2\pi}\sqrt{\tilde{J}_{34}\tilde{J}_{43}} = \sqrt{-\left(\tilde{J}_{34}\right)^2} \geq 0 \tag{A44}$$

given by (3.27) in which the parameter μ is given by (3.25).

A.3.3. *Case 3*

The resonance (of order $n = 2$) between a fast mode and a slow mode is characterised by $\omega_1 - \omega_3 = 2$. If this resonant case is destabilising, its maximal growth rate is then of the form

$$\sigma_{mm} = \frac{\varepsilon}{2\pi}\left(\mathrm{Re}\,\alpha\right)_{max} = \frac{\varepsilon}{2\pi}\sqrt{\tilde{J}_{13}\tilde{J}_{31}}, \tag{A45}$$

where

$$\tilde{J}_{13} = \left(\boldsymbol{T}^{-1}\right)_{11}\left(H_{11}^{+}T_{13} + H_{14}^{+}T_{43}\right) + \left(\boldsymbol{T}^{-1}\right)_{12}\left(H_{21}^{+}T_{13} + H_{24}^{+}T_{43}\right), \tag{A46a}$$

$$\tilde{J}_{31} = \left(\boldsymbol{T}^{-1}\right)_{31}\left(H_{11}^{+}T_{11} + H_{14}^{+}T_{41}\right) + \left(\boldsymbol{T}^{-1}\right)_{32}\left(H_{21}^{+}T_{11} + H_{24}^{+}T_{41}\right). \tag{A46b}$$

With the aid of (A11), (A12) and (A31) we find

$$\tilde{J}_{13} = \frac{\mathrm{i}\pi(1-\mu^2)}{8\omega_3(\omega_1^2-\omega_3^2)}\left(\left(4-\mathcal{N}^2\right)\omega_3^2 + \mathcal{B}^2\mathcal{N}^2\mu^2\right)\left(\omega_1 - \frac{\omega_1\omega_3^2}{\mathcal{B}^2\mu^2} + 2\mu^2\right), \tag{A47a}$$

$$\tilde{J}_{31} = \frac{\mathrm{i}\pi(1-\mu^2)}{8\omega_1(\omega_3^2-\omega_1^2)}\left(\left(4-\mathcal{N}^2\right)\omega_1^2 + \mathcal{B}^2\mathcal{N}^2\mu^2\right)\left(\omega_3 - \frac{\omega_3\omega_1^2}{\mathcal{B}^2\mu^2} - 2\mu^2\right). \tag{A47b}$$

We set

$$\mathcal{A}_0 = -\frac{(1-\mu^2)}{\left(\omega_1^2-\omega_3^2\right)^2}, \tag{A48a}$$

$$\mathcal{A}_1 = \left(\left(4-\mathcal{N}^2\right)\omega_3^2 + \mathcal{B}^2\mathcal{N}^2\mu^2\right)\left(\left(4-\mathcal{N}^2\right)\omega_1^2 + \mathcal{B}^2\mathcal{N}^2\mu^2\right), \tag{A48b}$$

$$\mathcal{A}_2 = \frac{(1-\mu^2)}{\omega_1\omega_3}\left(\omega_1 - \frac{\omega_1\omega_3^2}{\mathcal{B}^2\mu^2} + 2\mu^2\right)\left(\omega_3 - \frac{\omega_3\omega_1^2}{\mathcal{B}^2\mu^2} - 2\mu^2\right), \tag{A48c}$$

so as

$$\tilde{J}_{13}\tilde{J}_{31} = \frac{\pi^2}{64}\mathcal{A}_0\mathcal{A}_1\mathcal{A}_2. \tag{A49}$$

To calculate the quantities $\mathcal{A}_0$, $\mathcal{A}_1$ and $\mathcal{A}_2$ we proceed as follows. We use the resonance condition either in the form $\omega_1 - \omega_3 = 2$ or in an equivalent form (see (3.34))

$$1 - \mu^2 = \frac{16}{\left(4-\mathcal{N}^2\right)^2}\mathcal{B}^2\mu^2 \tag{A50}$$

together with the expressions of ω_1 and ω_3 described by (3.3) and determine $\omega_1\omega_3$, $\omega_1^2+\omega_3^2$ and $(\omega_1^2-\omega_3^2)^2$

$$\omega_1\omega_3 = -\frac{\left(4+\mathcal{N}^2\right)}{\left(4-\mathcal{N}^2\right)}\mathcal{B}^2\mu^2, \tag{A51a}$$

$$\omega_1^2+\omega_3^2 = 2\left(2+\omega_1\omega_3\right), \tag{A51b}$$

$$\left(\omega_1^2-\omega_3^2\right)^2 = 16\left(1+\omega_1\omega_3\right). \tag{A51c}$$

We therefore substitute (A51) into (A48) to obtain

$$\mathcal{A}_0 = -\frac{\mathcal{B}^2}{\left(4-\mathcal{N}^2\right)^2+\mathcal{B}^2\mathcal{N}^4}, \tag{A52a}$$

$$\mathcal{A}_1 = \left(4-\mathcal{N}^2\right)^3\left(1-\mu^2\right)\left[\left(4-\mathcal{N}^2\right)\left(1-\mu^2\right)+4\mathcal{N}^2\right], \tag{A52b}$$

$$\mathcal{A}_2 = -\frac{\left(1-\mu^2\right)}{\mathcal{B}^2\left(4+\mathcal{N}^2\right)}\left[\left(4-\mathcal{N}^2\right)\left(1-\mu^2\right)+4\mathcal{N}^2\right]. \tag{A52c}$$

Thus, we deduce the expression of σ_{mm}/ε given by (3.35).

References

Aravind, H.M., Dubos, T. & Mathur, M. 2022 Local stability analysis of homogeneous and stratified Kelvin–Helmholtz vortices. *J. Fluid Mech.* **943**, A18.

Bajer, K. & Mizerski, K.A. 2013 Elliptical flow instability in a conducting fluid triggered by an external magnetic field. *Phys. Rev. Lett.* **110**, 104503.

Balbus, S.A. & Hawley, J.F. 1991 A powerful local shear instability in weakly magnetized disks. I. Linear analysis. *Astrophys. J.* **376**, 214–222.

Barker, A.J. & Lithwick, Y. 2013 Non-linear evolution of the tidal elliptical instability in gaseous planets and stars. *Mon. Not. R. Astron. Soc.* **435** (4), 3614–3626.

Barker, A.J., Braviner, H.J. & Ogilvie, G.I. 2016 Non-linear tides in a homogeneous rotating planet or star: global modes and elliptical instability. *Mon. Not. R. Astron. Soc.* **459** (1), 924–938.

Barker, A.J. 2016 Non-linear tides in a homogeneous rotating planet or star: global simulations of the elliptical instability. *Mon. Not. R. Astron. Soc.* **459** (1), 939–956.

Barker, A.J. & Lithwick, Y. 2014 Non-linear evolution of the elliptical instability in the presence of weak magnetic fields. *Mon. Not. R. Astron Soc.* **437** (1), 305–315.

Bayly, B.J. 1986 Three-dimensional instability of elliptical flow. *Phys. Rev. Lett.* **57** (17), 2160–2163.

Benkacem, N., Salhi, A., Khlifi, A., Nasraoui, S. & Cambon, C. 2022 Destabilizing resonances of precessing inertia-gravity waves. *Phys. Rev.* E **105** (3), 035107.

Cambon, C. 1982 Etude spectrale d'un champ turbulent incompressible, soumis à des effets couplés de déformation et de rotation, imposés extérieurement. Doctoral dissertation, Université Claude Bernard-Lyon I, Villeurbanne.

Cambon, C., Teissedre, C. & Jeandel, D. 1985 Etude d'effets couplés de déformation et de rotation sur une turbulence homogène. *J. Méc.* **4** (5), 629–657.

Cébron, D., Le Bars, M., Le Gal, P., Moutou, C., Leconte, J. & Sauret, A. 2013 Elliptical instability in hot Jupiter systems. *Icarus* **226** (2), 1642–1653.

Chang, C. & Smith, S.G.L. 2021 Density and surface tension effects on vortex stability. Part 2. Moore–Saffman–Tsai–Widnall instability. *J. Fluid Mech.* **913**, A15.

Chandrasekhar, S. 1961 *Hydrodynamic and Hydromagnetic Stability*. Clarendon.

Chagelishvili, G.D., Zahn, J.P., Tevzadze, A.G. & Lominadze, J.G. 2003 On hydrodynamic shear turbulence in Keplerian discs: via transient growth to bypass transition. *Astron. Astrophys.* **402**, 401–407.

Craik, A.D.D. & Criminale, W.O. 1986 Evolution of wave-like disturbances in shear flows. A class of exact-solutions of the Navier–Stokes equations. *Proc. R. Soc. Lond.* A **406**, 13–26.

CRAIK, A.D.D. 1989 The stability of unbounded two- and three-dimensional flows subject to body forces: some exact solutions. *J. Fluid Mech.* **198**, 275–292.

CROW, S.C. 1970 Stability theory for a pair of trailing vortices. *AIAA J.* **8** (12), 2172–2179.

DAVIDSON, P.A. 2013 *Turbulence in Rotating, Stratified and Electrically Conducting Fluids*. Cambridge University Press.

ÉLOY, C. & LE DIZES, S. 2001 Stability of the Rankine vortex in a multipolar strain field. *Phys. Fluids* **13** (3), 660–676.

FEYS, J. & MASLOWE, S.A. 2016 Elliptical instability of the Moore–Saffman model for a trailing wingtip vortex. *J. Fluid Mech.* **803**, 556–590.

FUKUMOTO, Y. 2003 The three-dimensional instability of a strained vortex tube revisited. *J. Fluid Mech.* **493**, 287–318.

GLEDZER, E.B., DOLZHANSKY, F.V., OBUKHOV, A.M. & PONONMAREV, V.M. 1975 An experimental and theoretical study of the stability of a liquid in an elliptical cylinder. *Isv. Atmos. Ocean. Phys.* **11**, 617–622.

GODEFERD, F.S., CAMBON, C. & LEBLANC, S. 2001 Zonal approach to centrifugal, elliptic and hyperbolic instabilities in Stuart vortices with external rotation. *J. Fluid Mech.* **449**, 1–37.

GUIMBARD, D., LE DIZÈS, S., LE BARS, M., LE GAL, P. & LEBLANC, S. 2010 Elliptic instability of a stratified fluid in a rotating cylinder. *J. Fluid Mech.* **660**, 240–257.

HERREMAN, W., CÉBRON, D., LE DIZÈS, S. & LE GAL, P. 2010 Elliptical instability in rotating cylinders: liquid metal experiments under imposed magnetic field. *J. Fluid Mech.* **661**, 130–158.

KELVIN, L. 1887 Stability of fluid motion: rectilinear motion of viscous fluid between two parallel plates. *Phil. Mag.* **24** (5), 188–196.

KERSWELL, R.R. 1993*a* The instability of precessing flow. *Geophys. Astrophys. Fluid Dyn.* **72** (1–4), 107–144.

KERSWELL, R.R. 1993*b* Elliptical instabilities of stratified, hydromagnetic waves. *Geophys. Astrophys. Fluid Dyn.* **71** (1–4), 105–143.

KERSWELL, R.R. 1994 Tidal excitation of hydromagnetic waves and their damping in the Earth. *J. Fluid Mech.* **274**, 219–241.

KERSWELL, R.R. 2002 Elliptical instability. *Annu. Rev. Fluid Mech.* **34**, 83–113.

KUCHMENT, P.A. 1993 *Floquet Theory for Partial Differential Equations*, vol. 60. Springer.

LANDMAN, M.J. & SAFFMAN, P.G. 1987 The three-dimensional instability of strained vortices in a viscous fluid. *Phys. Fluids* **30** (8), 2339–2342.

LE BARS, M. & LE DIZÈS, S. 2006 Thermo-elliptical instability in a rotating cylindrical shell. *J. Fluid. Mech.* **563**, 189–198.

LEBOVITZ, N.R. & ZWEIBEL, E. 2004 Magnetoelliptic instabilities. *Astrophys. J.* **609**, 301–312.

LE REUN, T., FAVIER, B. & LE BARS, M. 2019 Experimental study of the nonlinear saturation of the elliptical instability: inertial wave turbulence versus geostrophic turbulence. *J. Fluid Mech.* **879**, 296–326.

LESUR, G. & PAPALOIZOU, J.C.B. 2009 On the stability of elliptical vortices in accretion discs. *Astron. Astrophys.* **498**, 1–12.

LEWEKE, T., LE DIZES, S. & WILLIAMSON, C.H. 2016 Dynamics and instabilities of vortex pairs. *Annu. Rev. Fluid Mech.* **48**, 507–541.

LIFSCHITZ, A. & HAMEIRI, E. 1991 Local stability conditions in fluid dynamics. *Phys. Fluids* A **3** (11), 2644–2651.

LIFSCHITZ, A. 1994 On the stability of certain motions of an ideal incompressible fluid. *Adv. Appl. Maths* **15**, 404–436.

MALKUS, W.V.R. 1989 An experimental study of the global instabilities due to the tidal (elliptical) distortion of a rotating elastic cylinder. *Geophys. Astrophys. Fluid Dyn.* **48**, 123–134.

MCKEOWN, R., OSTILLA-MÓNICO, R., PUMIR, A., BRENNER, M.P. & RUBINSTEIN, S.M. 2020 Turbulence generation through an iterative cascade of the elliptical instability. *Sci. Adv.* **6** (9), eaaz2717.

MIZERSKI, K.A. & BAJER, K. 2009 The magnetoelliptic instability of rotating systems. *J. Fluid Mech.* **632** (1), 401–430.

MIZERSKI, K.A. & LYRA, W. 2012 On the connection between the magneto-elliptic and magneto-rotational instabilities. *J. Fluid Mech.* **698**, 358–373.

MIYAZAKI, T. 1993 Elliptical instability in a stably stratified rotating fluid. *Phys. Fluids* A **5** (11), 2702–2709.

MIYAZAKI, T. & FUKUMOTO, Y. 1992 Three-dimensional instability of strained vortices in a stably stratified fluid. *Phys. Fluids* A **4** (11), 2515–2522.

MOFFATT, H.K. 2010 Note on the suppression of transient shear-flow instability by a spanwise magnetic field. *J. Engng Maths* **68**, 263–268.

MOORE, D.W. & SAFFMAN, P.G. 1975 The instability of a straight vortex filament in a strain field. *Proc. R. Soc. Lond.* A **346**, 413–425.

NORNBERG, M.D., JI, H., SCHARTMAN, E., ROACH, A. & GOODMAN, J. 2010 Observation of magnetocoriolis waves in a liquid metal Taylor–Couette experiment. *Phys. Rev. Lett.* **104** (7), 074501.

OGILVIE, G.I. 2014 Tidal dissipation in stars and giant planets. *Annu. Rev. Astron. Astrophys.* **52**, 171–210.

OTHEGUY, P., CHOMAZ, J.M. & BILLANT, P. 2006 Elliptic and zigzag instabilities on co-rotating vertical vortices in a stratified fluid. *J. Fluid Mech.* **553**, 253–272.

PEDLOSKY, J. 2013 *Geophysical Fluid Dynamics*. Springer.

PIERREHUMBERT, R.T. 1986 Universal short-wave instability of two-dimensional eddies in an inviscid fluid. *Phys. Rev. Lett.* **57** (17), 2157–2159.

SAGAUT, P. & CAMBON, C. 2008 *Homogeneous Turbulence Dynamics*. Cambridge University Press.

SCHECTER, D.A., BOYD, J.F. & GILMAN, P.A. 2001 "Shallow-water" magnetohydrodynamic waves in the Solar tachocline. *Astrophys. J.* **551** (2), L185.

SALHI, A. & CAMBON, C. 1997 An analysis of rotating shear flow using linear theory and DNS and LES results. *J. Fluid Mech.* **347**, 171–195.

SALHI, A. & CAMBON, C. 2009 Precessing rotating flows with additional shear: stability analysis. *Phys. Rev.* E **79** (3), 036303.

SALHI, A., LEHNER, T. & CAMBON, C. 2010 Magnetohydrodynamic instabilities in rotating and precessing sheared flows: an asymptotic analysis. *Phys. Rev.* E **82** (1), 016315.

SALHI, A., LEHNER, T., GODEFERD, F. & CAMBON, C. 2012 Magnetized stratified rotating shear waves. *Phys. Rev.* E **85** (2), 026301.

SALHI, A., BAKLOUTI, F.S., GODEFERD, F., LEHNER, T. & CAMBON, C. 2017 Energy partition, scale by scale, in magnetic Archimedes Coriolis weak wave turbulence. *Phys. Rev.* E **95** (2), 023112.

SALHI, A., KHLIFI, A. & CAMBON, C. 2020 Nonlinear effects on the precessional instability in magnetized turbulence. *Atmosphere* **11** (1), 14.

SINGH, S. & MATHUR, M. 2019 Effects of Schmidt number on the short-wavelength instabilities in stratified vortices. *J. Fluid Mech.* **867**, 765–803.

SIPP, D., LAUGA, E. & JACQUIN, L. 1999 Vortices in rotating systems: centrifugal, elliptic and hyperbolic type instabilities. *Phys. Fluids* **11** (12), 3716–3728.

SIPP, D. & JACQUIN, L. 2003 Widnall instabilities in vortex pairs. *Phys. Fluids* **15**, 1861–1874.

SLANE, J. & TRAGESSER, S. 2011 Analysis of periodic nonautonomous inhomogeneous systems. *Nonlinear Dyn. Syst. Theory* **11** (2), 183–198.

SUZUKI, S., HIROTA, M. & HATTORI, Y. 2018 Strato-hyperbolic instability: a new mechanism of instability in stably stratified vortices. *J. Fluid Mech.* **854**, 293–323.

TSAI, C.Y. & WIDNALL, S.E. 1976 The stability of short waves on a straight vortex filament in a weak externally imposed strain field. *J. Fluid Mech.* **73** (4), 721–733.

WALEFFE, F. 1989 The 3-D instability of a strained vortex and its relation to turblence. PhD thesis, Massachusetts Institute of Technology, Cambridge, MA.

WALEFFE, F. 1990 On the three-dimensional instability of strained vortices. *Phys. Fluids* A **2** (1), 76–80.

WALEFFE, F. 1992 The nature of triad interactions in homogeneous turbulence. *Phys. Fluids* A **4** (2), 350–363.

WANG, Y., GILSON, E.P., EBRAHIMI, F., GOODMAN, J. & JI, H. 2022 Observation of axisymmetric standard magnetorotational instability in the laboratory. *Phys. Rev. Lett.* **129** (11), 115001.

WILCZYŃSKI, F., HUGHES, D.W. & KERSALÉ, E. 2022 Magnetic buoyancy instability and the anelastic approximation: regime of validity and relationship with compressible and Boussinesq descriptions. *J. Fluid Mech.* **942**, A46.

ZWIRNER, L., TILGNER, A. & SHISHKINA, O. 2020 Elliptical instability and multiple-roll flow modes of the large-scale circulation in confined turbulent Rayleigh–Bénard convection. *Phys. Rev. Lett.* **125** (5), 054502.